IOP PUBLISHING REPORTS ON PROGRESS IN PHYSICS

Rep. Prog. Phys. **76** (2013) 076901 (21pp) doi:10.1088/0034-4885/76/7/076901

Lunar laser ranging: the millimeter challenge

T W Murphy

Center for Astrophysics and Space Sciences, University of California, San Diego, 9500 Gilman Drive, La Jolla, CA 92093-0424, USA

E-mail: tmurphy@physics.ucsd.edu

Received 17 December 2010, in final form 18 February 2013
Published 14 June 2013
Online at stacks.iop.org/RoPP/76/076901

Abstract

Lunar laser ranging has provided many of the best tests of gravitation since the first Apollo astronauts landed on the Moon. The march to higher precision continues to this day, now entering the millimeter regime, and promising continued improvement in scientific results. This review introduces key aspects of the technique, details the motivations, observables, and results for a variety of science objectives, summarizes the current state of the art, highlights new developments in the field, describes the modeling challenges, and looks to the future of the enterprise.

(Some figures may appear in colour only in the online journal)

This article was invited by Beverly K Berger.

Contents

1. The LLR concept

Since 1969, lunar laser ranging (LLR) has provided high-precision measurements of the Earth–Moon distance, contributing to the foundations of our knowledge in gravitation and planetary physics. While being the most evident force of nature, gravity is in fact the weakest of the fundamental forces, and consequently the most poorly tested by modern experiments. Einstein's general relativity (GR)—currently our best description of gravity—is fundamentally incompatible with quantum mechanics and is likely to be replaced by a more complete theory in the future. A modified theory would, for example, predict small deviations in the solar system that, if seen, could have profound consequences for understanding the universe as a whole.

Utilizing reflectors placed on the lunar surface by American astronauts and Soviet rovers, LLR measures the round-trip travel time of short pulses of laser light directed

to one reflector at a time (figure 1). By mapping the shape of the lunar orbit, LLR is able to distinguish between competing theories of gravity. Range precision has improved from a few decimeters initially to a few millimeters recently, constituting a relative precision of 10^{-9}–10^{-11}. Leveraging the raw measurement across the Earth–Sun distance provides another two orders of magnitude for gauging relativistic effects in the Earth–Moon–Sun system.

As LLR precision has improved over time, the technique has remained at the cutting edge of tests of gravitational phenomenology and probes of the lunar interior, and has informed our knowledge of Earth orientation, precession, and coordinate systems. LLR was last reviewed in this series in 1982 [1]; this update describes the key science drivers and findings of LLR, the apparatus and technologies involved, the requisite modeling techniques, and future prospects on all fronts. LLR is expected to continue on its trajectory of improvement, maintaining a leading role in contributions to science. Other recent reviews by Merkowitz [2] and by Müller *et al* [3] complement the present one. The Merkowitz review, like this one, stresses gravitational tests of LLR, but with greater emphasis on associated range signals. Next-generation reflector and transponder technologies are more thoroughly covered. The Müller *et al* review (for which this author is a co-author) offers a more complete history of LLR, has statistics on the LLR data set, and provides greater emphasis on geophysics, selenophysics, and coordinate systems.

This review is organized as follows: section 1 provides an overview of the subject; section 2 reviews the science delivered by LLR, with an emphasis on gravitation; section 3 describes current LLR capabilities; section 4 relates recent surprises from LLR, including the finding of the lost Lunokhod 1 reflector and evidence for dust accumulation on the reflectors; section 5 treats the modeling challenges associated with millimeter-level LLR accuracy; and section 6 offers possible future directions for the practice of LLR. An appendix contains a list of acronyms used in the text. Some single-use ancillary acronyms are only defined in the appendix in order to minimize unimportant interruptions.

1.1. Current science results

A detailed description of the science capabilities of LLR is deferred until section 2. For the purposes of introducing the motivation behind the effort, LLR provides the following leading tests and measurements

- the strong equivalence principle (EP) to $\eta \approx 3 \times 10^{-4}$ sensitivity [4, 5];
- time-rate-of-change of the gravitational constant to $\dot{G}/G < 10^{-12}\,\mathrm{yr}^{-1}$ [6–8];
- geodetic precession within 0.3% of GR prediction [3];
- gravitomagnetism within ∼0.2% of GR prediction [9, 10];
- the $1/r^2$ law to $\sim 2 \times 10^{-11}$ times the strength of gravity at 10^8 m scales [11, 12];
- the presence of a liquid core in the Moon having a radius of ∼350 km [13, 14].

Figure 1. Lunar Laser Ranging in action at the Apache Point Observatory in southern New Mexico. Photo by Dan Long.

LLR also provides checks on preferred-frame effects [15, 16], and Newton's third law [17]. LLR may additionally open a window into the possible existence of extra dimensions via cosmological dilution of gravity [18, 19]. Besides the strong EP (SEP), LLR tests the weak EP (WEP) at the level of $\Delta a/a < 1.3 \times 10^{-13}$ [20]. Laboratory tests of the WEP reach similar levels [21], but result in more incisive tests by having the freedom to choose more optimal mass pairs than the iron-silicate pairing dictated by the Earth–Moon system. Finally, LLR is used to define coordinate systems, probe the lunar interior, and study geodynamics [22]. Order-of-magnitude advances in each of these domains is possible as the LLR technique improves from the centimeter to the millimeter regime.

1.2. A quantitative introduction

By way of introduction, this section presents representative numbers meant to portray key aspects of the LLR technique. Some items will enter in subsequent discussion, while others appear only here for the sake of overall familiarity.

While the semi-major axis of the lunar orbit is 384 402 km, the time-averaged distance between Earth and Moon centers is 385 000.6 km, corresponding to 2.56 s of round-trip light travel time. The range varies from 356 500 to 406 700 km, chiefly due to a 21 000 km amplitude oscillation (27.55 d period) associated with the elliptical orbit of the Moon ($e = 0.055$). Other leading oscillations appear at 3700 km (31.8 d) and 2955 km (14.76 d) due to solar perturbations. The range rate between Earth and Moon centers may be as large as 75 m s^{-1}, while Earth rotation is the dominant range-rate effect, measuring 465 m s^{-1} at the equator.

The basic arrangement for performing LLR is shown in figure 2. Illuminating the reflectors sufficiently is a principal challenge in LLR. Even a 1 arcsec (5 μrad) beam—limited by atmospheric turbulence—spreads to 1.9 km at the lunar surface. This translates into a one-in-25-million chance of a photon launched from Earth finding the Apollo 11 reflector, for instance (discussed in section 1.3). The return journey

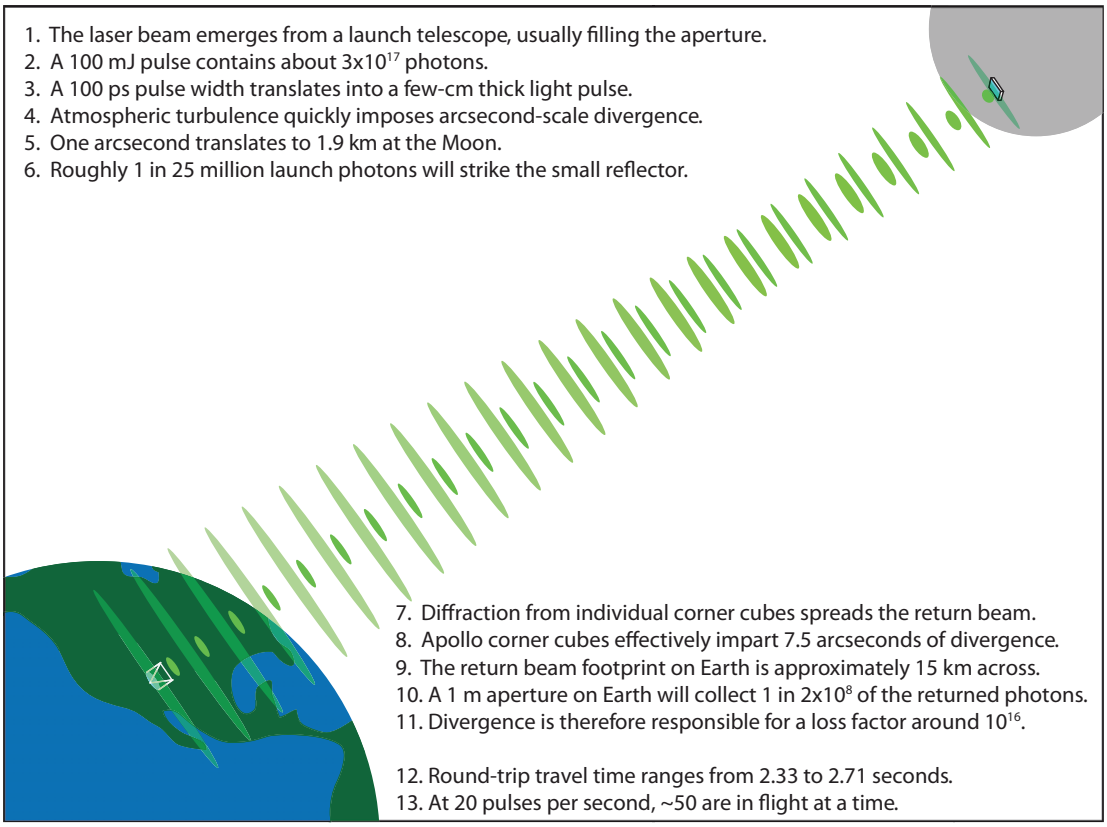

Figure 2. Cartoon schematic of LLR technique and divergence-related challenges.

is even more difficult, owing to diffractive spread from the corner cube prisms, compounded by velocity aberration. A 1 m circular aperture on Earth can expect to receive one photon out of every 250 million emerging from the Apollo reflector. The tangential relative motion of the Earth station with respect to the Moon introduces a 4–6 μrad velocity aberration, translating to a $\sim$2 km offset of the return pattern on the Earth's surface and a further reduction of the Apollo reflector signal by a factor of 0.6–0.8.

A useful conversion to memorize is that 1 mm of separation translates into 6.67 ps of round-trip travel time, or inversely 1 ns of round-trip time maps to 0.15 m of one-way distance.

1.3. Reflectors and divergence-imposed requirements

We now review the instruments on the Moon and the requirements they impose on the ground apparatus. Example performance is also presented in section 3.2.

LLR relies on a total of five passive reflectors left on the surface of the Moon roughly 40 years ago (figure 3). The Apollo arrays—landed on the Apollo 11, Apollo 14, and Apollo 15 missions—consist of, respectively, 100, 100 and 300 3.8 cm diameter fused silica corner cube reflectors employing total internal reflection. The Luna 17 and Luna 21 Soviet missions to the Moon landed the Lunokhod 1 and Lunokhod 2 rovers, each carrying identical reflector arrays built by the French. These arrays consist of 14 corner cubes each having a triangular edge length of 11 cm and silvered rear surfaces. The

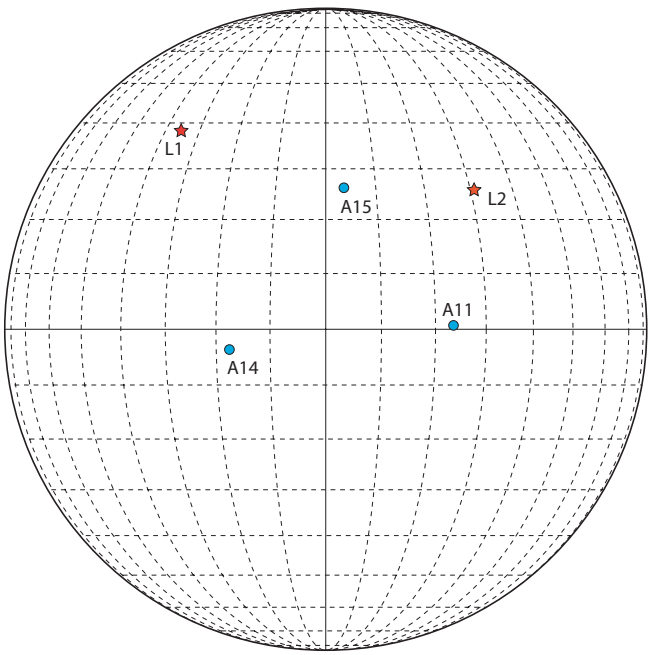

Figure 3. Positions of the five reflectors on the lunar surface. "A" stands for Apollo, while "L" stands for Lunokhod.

nominal response of the Lunokhod arrays falls between that of the 100-element and 300-element Apollo arrays. Pictures of both types of arrays appear in figure 4.

Lunar libration changes the apparent tilt of the reflectors with respect to the Earth–Moon line of sight, seen in figure 5

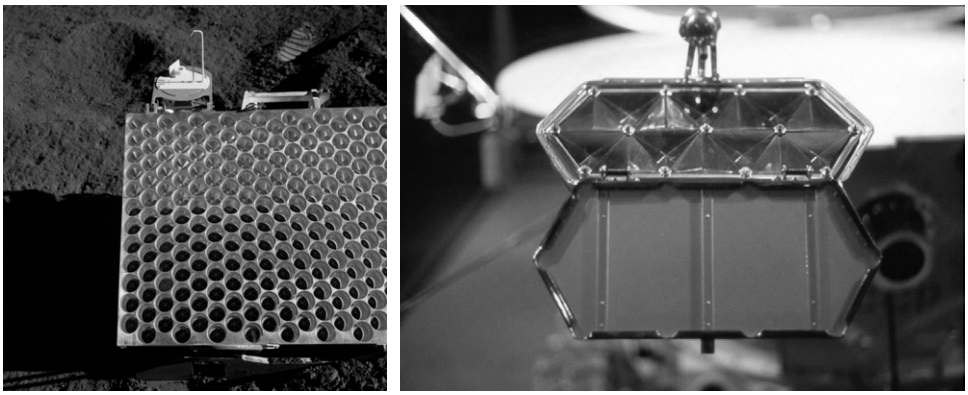

Figure 4. A portion of the Apollo 15 reflector (left; courtesy NASA), consisting of 300 corner cube reflectors each 3.8 cm in diameter. All Apollo reflectors are mounted in a similar aluminum tray, except that the Apollo 11 and Apollo 14 reflectors are 100-element arrays arranged in a 10×10 square pattern. At right is the Lunokhod reflector design (courtesy the Lavochkin Association).

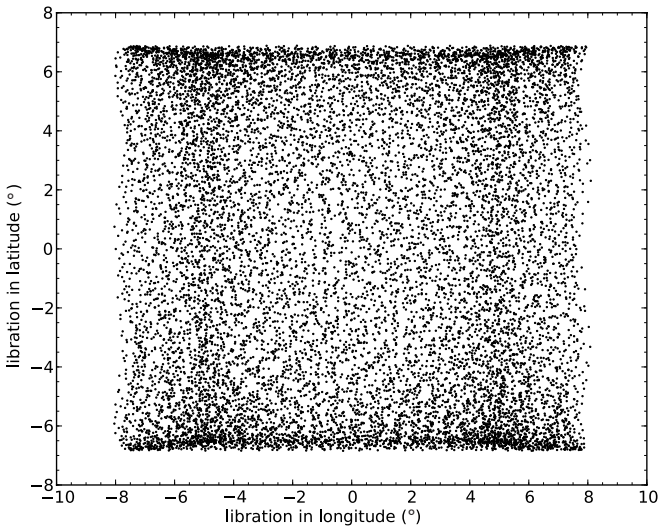

Figure 5. Libration pattern for the Moon over 18.6 years, at 12 h samples.

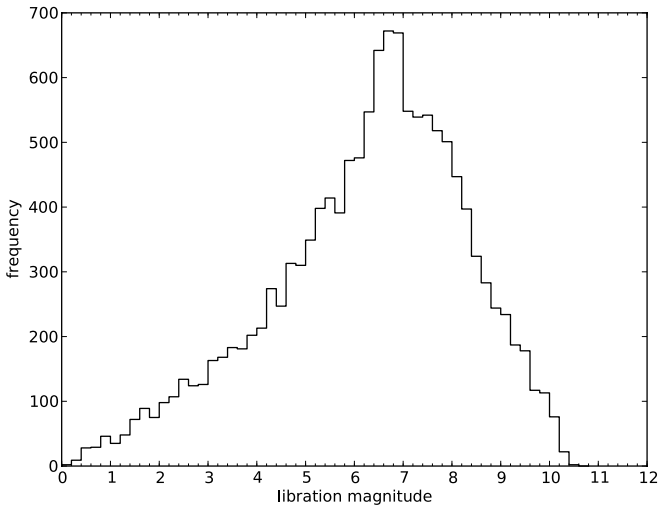

Figure 6. Total libration frequency histogram, ignoring topocentric contributions.

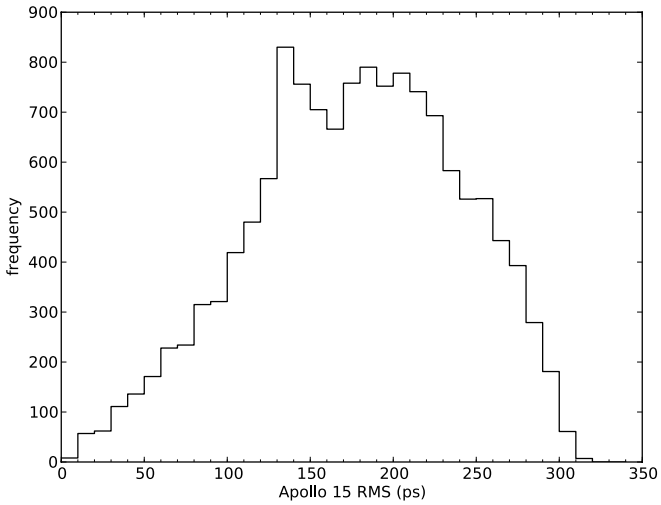

Figure 7. Impact of librations on the RMS temporal variation contributed by the Apollo 15 reflector.

filling out a rectangle spanning ±8.1° in longitude and ±6.9° in latitude—not including the Earth topocentric correction, which can modify effective libration by as much as a degree. The median total libration is 6.5°, and can be in excess of 10° (figure 6), again ignoring topocentric considerations. As a result, the return pulse acquires a temporal spread due to the fact that some corner cube reflectors are closer to the observer, while others are farther. For the Apollo 15 array, the full-width at half-maximum (FWHM) can approach 1 ns (150 mm one-way), or a root-mean-square (RMS) in excess of 300 ps (figure 3). A typical case of 200 ps RMS corresponds to 30 mm of one-way distance, and thus requires 900 measurements (photons) in order to achieve a statistical uncertainty in the neighborhood of 1 mm. Thus precision LLR demands hundreds or thousands of photons in order to overcome the libration/reflector-imposed measurement uncertainty.

The signal loss in the two-way laser link is staggeringly high, generally amounting to a loss factor in the neighborhood of 10^{18}. Beam divergence on both the up-leg and down-leg result in a signal strength that depends on the inverse-fourth power of distance.

The up-leg divergence is limited by atmospheric turbulence (seeing), so that one may not generally expect better than about 1 arcsec (5 μrad) divergence, translating to about 4×10^{-8} throughput onto the smaller Apollo 11 and

14 arrays. The down-leg divergence is set by diffraction from the corner cubes. Total internal reflection corner cubes like those used for Apollo produce a central irradiance that is 0.15 times that of a simplistic top-hat illumination pattern of angular diameter λ/D, where λ is the wavelength and D is the corner cube diameter. The result is that a 1 m circular aperture on Earth receives about 5×10^{-9} of the flux incident on the reflector at a wavelength of 532 nm. The net throughput is then $\sim 2 \times 10^{-16}$ for a 1 m aperture, scaling as a^2/λ^2, where a is the aperture diameter. Multiplying by typical optical system and atmospheric throughputs (traversed twice), together with filter transmissions and detection efficiencies, total throughput tends to be in the range of 10^{-18}. An energetic pulse of laser light having a pulse width in the neighborhood of 100 ps might be 100 mJ, containing 3×10^{17} photons at green wavelengths. The result is that LLR invariably operates in the single-photon detection regime.

The ground apparatus therefore benefits from having

- a powerful laser, typically a few watts, with substantial pulse energy;
- sub-arcsecond intrinsic divergence, meaning a launch beam diameter exceeding 10 cm;
- sub-arcsecond pointing and tracking capability;
- a large collection aperture for the return;
- aggressive filtering in the temporal, spatial, and wavelength domains.

Additionally, the laser pulsewidth should be <100 ps so that it does not compete with the reflector-induced spread in the overall error budget. Many of the requirements are naturally satisfied by using an astronomical telescope as both the launch and receive instrument in a so-called mono-static arrangement. For perspective, a 1 W laser limited to 1 arcsec divergence by the atmosphere will return approximately 10^{-16} W m^{-2} to the ground, translating to a 19th magnitude source viewed through a 100 nm wide broadband filter. Meanwhile, the full moon reaches −13 mag, or about 10^{13} times brighter. More fairly, the surface brightness of the full moon is about 3 mag arcsec^{-2}, so that an aperture (spatial filter) spanning four square arcseconds admits 10^7 times more background than signal, or a signal-to-background ratio (SBR) around 10^{-7}. A wavelength filter having a 1 nm passband increases the SBR to $\sim 10^{-5}$, and temporal filtering at the 1 ns level compared to a 50 ms repetition rate (20 Hz) carries a factor of 5×10^7 for a net SBR ≈500. Clearly, the temporal filter is the most effective of the three. Missing from this discussion is the apparent degradation of the lunar reflector response [23], reduced by a factor of ten across the board, and an additional factor of ten at full moon (discussed in section 4.2).

An example return from Apollo 15 is shown in figure 8, demonstrating the effect of libration as well as the high SBR recently achieved in LLR measurements. A histogram of the same data is presented in figure 9, in which it is seen that the temporal width of the lunar return is almost completely determined by the libration-induced reflector spread. Details on the apparatus used to acquire these data can be found in section 3.2.

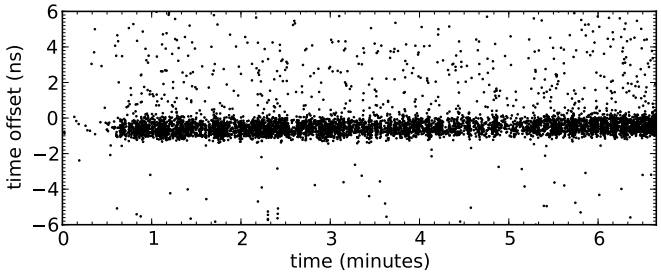

Figure 8. 8000-shot measurement to Apollo 15 on 2010 March 23, showing a 12 ns portion of the 100 ns return window. This is the first run of the night, demonstrating a typical fast acquisition and optimization of the signal. Background photons and detector dark events are scattered below (before) the lunar return. A diffusion process in the detector contributes to a "tail" of late responses after the lunar return. It is typical for the timing of the return to differ from an approximate prediction by ∼1 ns, as seen here. The temporal thickness of the Apollo 15 return is due to the finite size of the slightly tilted reflector, as seen more clearly in figure 9.

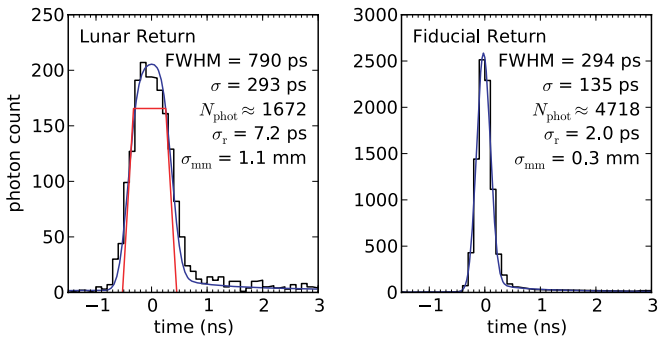

Figure 9. Histogram of the lunar return from figure 8 (left), along with a fiducial measurement reflecting the system performance (right). A functional fit to the fiducial return (from a local corner cube) is convolved with the trapezoidal shape resulting from the total libration—lunar plus Earth topocentric correction—at the time of observation to make the fit line for the lunar return. The FWHM and RMS of each distribution is given, along with the number of contributing photons and a measure of centroiding ability given by statistical reduction of the RMS by $\sqrt{N}$, expressed in picoseconds and millimeters.

1.4. Fundamental measurement and world lines

It is important to understand the fundamental measurement performed by LLR. After a brief description in this section, a more detailed treatment may be found in section 5.1. A stable clock provides a frequency reference by which time intervals may be precisely measured. Time transfer techniques—usually via the Global Positioning System (GPS)—guarantee long-term frequency stability and synchronization with atomic clock ensembles around the globe.

The core measurement consists of recording two event times—corresponding to photon launch and detection—against the local clock. The launch time is generally gauged by measuring the return from a local corner cube mounted at the telescope exit aperture, heavily attenuated to the single-photon level so that the same detector and timing system may be used for both the local (fiducial) and remote (lunar) photon returns. A constant offset between the Earth-fixed axis intersection of the telescope and fiducial corner cube is added to each range measurement. In order to achieve millimeter-level precision,

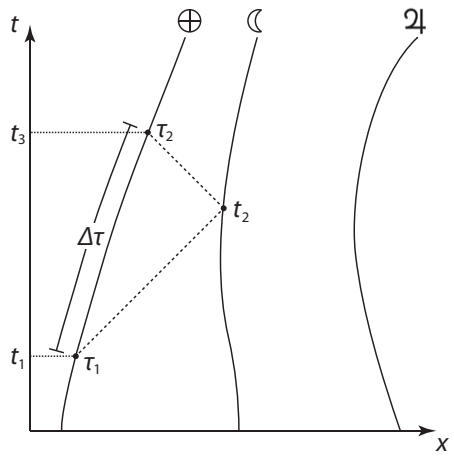

Figure 10. Schematic of fundamental LLR measurement. The Earth and Moon move through the SSB frame, influencing each other and being influenced by other solar system bodies (e.g. the Sun, Jupiter). A light pulse travels a null geodesic from the Earth to the Moon and back, while the Earth clock ticks off a proper time, $\Delta\tau = \tau_2 - \tau_1$. The event times are transformed into the SSB frame (t_1 and t_3) and the entire solar system model is adjusted (including the bounce time, t_2) until the various world lines are made to match the entire set of LLR measurements.

the *absolute* time only needs to be accurate at the microsecond level (Earth rotation modifies the Earth–Moon distance by ∼0.4 mm in 1 μs), while the *relative* time must be understood at the few-picosecond level. The latter requirement translates to frequency stability at the 10^{-12} level over the course of a few seconds.

Because all massive solar system bodies influence the Earth–Moon range, the analysis is most conveniently performed in the solar system barycenter (SSB) frame. The measured times are transformed into SSB coordinates using standard time transformation techniques—as outlined, for example, by Moyer [24]—primarily consisting of adjustments to account for velocity-induced time dilation and gravitational redshift resulting from the solar potential. Accounting for body figures and rotation of Earth and Moon (and the solar J_2), a fully relativistic (Einstein–Infeld–Hoffmann: EIH) equation of motion is numerically integrated, varying input parameters—chiefly initial conditions—to search for dynamical world-lines (figure 10) of the relevant bodies that satisfy the round-trip light propagation measurements in the SSB frame. Parameters in the relativistic model allowing departures from the specific prescription of GR indicate deviations from GR. The technique is more fully described [25, 26], and in section 5.1. Simultaneous numerical integration of lunar rotation is critical for computing consistent dynamics, and will be treated further in section 2.2.1.

2. Science from LLR

Here we present a more comprehensive account of the science delivered by LLR than was introduced in section 1.1. First, we look at gravitation, including the EP, time-rate-of-change of Newton's G, gravitomagnetism, geodetic precession, and the inverse-square law. Next, we briefly address the lunar interior and geophysical concerns.

2.1. Relativity and gravity

The concordance of astrophysical measurements in the last 15 years—the anisotropy scale of the cosmic microwave background [27–31], the distance measurements of type Ia supernovae [32, 33], the gravitational behaviors of galactic superclusters [34], and the power spectrum of large-scale structure [35]—point to the surprising conclusion that the expansion of the universe is *accelerating*, implying some form of a *fundamentally new* gravitational phenomenon. The cosmological acceleration could be due to a scalar field that produces effects similar to those associated with the 'cosmological constant,' originally introduced into the relativistic field equations by Einstein. A scalar field would likely couple to the gravitational field in such a way as to produce a departure from the EP [36], and would introduce time variations in the fundamental coupling constants of nature [37]. EP and $\dot{G}$ tests therefore have discovery potential with a very broad reach, and in fact provide some of the most sensitive low-energy probes for new physics. In light of recent discoveries, it is important that scientific inquiry is not restricted to current theoretical expectations, but rather that every available avenue for testing the nature of gravity is examined.

The lunar orbit offers a pristine laboratory for testing gravity, as non-gravitational effects on the orbit begin to show up only at the millimeter level. Moreover, the Moon is far enough from the Earth to be dominated by solar gravity, so that the Earth and Moon may each be considered to be in *solar* orbits. This fact makes the Earth–Moon–Sun system useful as a probe of the EP (and other relativistic phenomena) at scales of 1 AU—extending the baseline against which to compare the raw measurement precision.

We highlight here some of the contributions to gravitational physics from LLR. The list is not complete, but provides a sense of the cornerstone capabilities. Most of these science results are based on modeling that currently produces post-fit residuals of measured data in the neighborhood of 2 cm, so that millimeter-quality data could in principle improve current limits by an order of magnitude given commensurate improvements in modeling (see section 5).

2.1.1. Equivalence principle. The simplest prediction of Einstein's EP—the universality of free fall—is one of the most precisely tested principles in all of physics. Yet there are strong motivations for extending the tests and pushing their precisions even higher. The EP can be decomposed into two key forms. The weak form of the EP (WEP) applies to the gravitational properties of all forms of mass–energy except for gravity, while the SEP extends the WEP to include gravity itself.

The Earth–Moon–Sun system is currently the *best available* probe of the SEP, first pointed out by Nordtvedt [38–40]. From the vantage point of the EP, the Earth and Moon are test bodies that differ in two important ways. First, the Earth's mass has a fractional contribution from gravitational self-energy (4.6×10^{-10}) that is about 20 times greater than the corresponding measure for the Moon—allowing LLR to test the SEP. Second, the Earth has a massive iron-nickel core

while the Moon does not—making LLR sensitive to a WEP violation as well. Laboratory EP tests of Earth-like and Moon-like objects falling toward the sun can be used to distinguish between an SEP and a WEP violation [21].

LLR tests the SEP by measuring the difference in the accelerations of the Earth and Moon toward the Sun. In the presence of a differential acceleration, the orbit of the Moon—from our perspective on the Earth—would appear to be displaced, or *polarized*, toward or away from the Sun. The range signal would take the form

$$\Delta r \cong 13\eta \cos D \text{ meters},$$

where $D = (\omega - \Omega)t$ is the lunar orbit's synodic phase[1] having a period of 29.53 days, with $D = 0$ corresponding to new moon [41]. The parameter η is a theory-dependent dimensionless coefficient *sensitive to almost every post-Newtonian feature of the theory*. Although η vanishes in GR, it generally does not in alternative theories. But independent of any theory, this test of the SEP addresses a very basic and important question—what is the weight of gravity itself? It tests a crucial non-linear property of gravity: how gravity produces energy that itself gravitates.

The metric models by Damour and Nordtvedt [42] describe a relaxation of scalar field strength that today would produce SEP differential accelerations between 5×10^{-17} and 10^{-13}. The present limit on differential acceleration is $\Delta a/a \approx \pm 1.3 \times 10^{-13}$ [4, 5, 20], corresponding to a test of the SEP at the level of $|\eta| < 3 \times 10^{-4}$, given the self-energy fraction of the Earth. Millimeter-quality ranging stands to improve sensitivity of the SEP test by one order of magnitude, measuring $\Delta a/a$ to a precision of $\pm 10^{-14}$ and reaching into the theoretically motivated range indicated above. The closest competitor comes from pulsars. A composite of 27 pulsars places a 1–σ limit on the SEP of 2.3×10^{-3}—roughly an order of magnitude shy of the LLR result [43, 44].

2.1.2. Time-rate-of-change of G. A secular change in the gravitational constant, G, would produce secular changes in the lunar mean distance and the orbital period (Kepler's third law), as well as in the angular rate of the Earth about the Sun. While the orbital radius change results in a range signal that varies linearly in time, the change in orbital period leads to a quadratic evolution of the Moon's mean anomaly (phase). It is this quadratic dependence that most powerfully constrains $\dot{G}$. Here, the long time span of LLR measurements becomes important, limiting $\dot{G}/G$ at the impressive level of 7×10^{-13} yr^{-1} [6] and 9×10^{-13} yr^{-1} [7]—the best available experimental results.

Recently Steinhardt and Wesley examined the constraints that observations and experiment place on a broad class of theories that attempt to explain dark energy in the context of extra dimensions [45]. They find that if current constraints on *both* $\dot{G}$ *and* the value and rate-of-change of the equation-of-state parameter, w, improve by a factor of two, such ideas could be ruled out at the 3σ level. In their analysis, Steinhardt and Wesley use a 1994 pulsar timing limit for $\dot{G}$ of 5×10^{-12}. LLR already exceeds this limit by an order of magnitude. A recent work questions the validity of several previous published pulsar limits on $\dot{G}/G$—including the 1994 result—finding instead trustworthy limits in the neighborhood of 20×10^{-12} yr^{-1} [46]. However, a new report puts forth a limit at 1.6×10^{-12} yr^{-1}, approaching levels tested by LLR [47].

2.1.3. Gravitomagnetism, geodetic precession, and other parametrized post-newtonian tests. LLR tests a number of basic relativistic phenomenologies—independent of whether gravity is described by a metric theory. These phenomena include gravitomagnetism, geodetic precession, and the consequences of preferred frames. Many such phenomena can be cast into the Parametrized Post-Newtonian (PPN) framework [48, 49]: a generalized metric description of gravity for which GR is a special case. The most prominent PPN parameters are γ, describing the amount of curvature produced per unit mass, and β, describing the non-linearity of gravity. Both of these are unity in GR. The best constraint on γ comes from Doppler ranging to Cassini: $|\gamma - 1| < 2.3 \times 10^{-5}$ [50]. β is best constrained by LLR tests of the SEP via the identity: $\eta \equiv 4\beta - \gamma - 3$. Combining the Cassini result for γ with the LLR result for η yields $|\beta - 1| < 1 \times 10^{-4}$ [20].

Preferred-frame effects, such as those codified by PPN parameters α_1 and α_2, are also tested by LLR, currently at the level of 9×10^{-5} and 2×10^{-5}, respectively [6, 15], although Nordtvedt obtains a 10^{-7} limit on α_2 based on the long-term orientation of the spin axis of the Sun [16].

Gravitomagnetism is a generic consequence of any mass in motion. As the Earth orbits the Sun, its gravitomagnetic field exerts a Lorentz force on the Moon. Eliminating the gravitomagnetic term from the EIH equations of motion would result in experimentally absent six-meter-amplitude periodic disturbances at both synodic and twice-synodic frequencies [9]. LLR constrains gravitomagnetism—the root of 'frame dragging'—to <0.2% precision, as confirmed by a covariant analysis [10]. Within the PPN context, gravitomagnetism reduces to non-competitive checks on parameters γ and α_1. By comparison, the Gravity Probe-B experiment obtained a final precision on the gravitomagnetic effect of 19% [51], and laser ranging to the LAGEOS satellites produce results in the 5–40% range [52, 53]. Pulsars may soon contribute gravitomagnetic limits as well, although no pulsar results have been published to date.

Gravitomagnetism, at its core, is a frame-dependent phenomenology. As such, the assertion that LLR is sensitive to gravitomagnetism has been questioned from the point of view that one may nullify the effect by performing LLR analysis in an Earth-centered frame [54, 55]. Leaving aside complications arising from the fact that the resulting frame is non-inertial (not asymptotically flat), the attempt to separate gravitomagnetism into 'intrinsic' and 'gauge-dependent' varieties is, in the author's view, as specious as it would be for the magnetic field of electromagnetism: there are not two physically distinct flavors of magnetic fields. A similar argument could be made that performing analysis of LAGEOS or Gravity Probe-B measurements of

[1] The synodic phase of the Moon describes its angle with respect to the Earth–Sun line, thus referring to the familiar illumination cycle of lunar phases.

Lense–Thirring or Schiff precessions, respectively, in a frame rotating with the Earth would likewise eliminate the source of gravitomagnetism. Obviously other frame-dependent phenomenologies should intercede to produce the same observational result, but this merely amplifies the notion of gravitomagnetism as part of the frame-transformation package. Keeping in mind that converting measurements into the SSB frame for LLR analysis reduces to a straightforward matter of time transformation, as summarized in section 1.4, the lack of anomalous gravitomagnetic signatures when evaluating LLR data in the context of the EIH equations of motion essentially stands as confirmation that gravitomagnetism plays its expected role in frame transformation [56]. The appearance of the PPN preferred-frame parameter, α_1, in the coefficient for the gravitomagnetic term in the equations of motion further clarifies this association.

Geodetic precession, also known as de Sitter precession, can be understood as the effect of parallel transport of a fixed direction—as manifested by a gyroscope or orbital axis, for instance—around the curved space surrounding a central body. The curvature results in a migration of the axis direction relative to the background inertial space upon completing an orbit. One revolution around the Sun at the distance of the Earth produces a directional offset of 19.2 marcsec. This precession rate in the orientation of the lunar orbit is confirmed by LLR [25, 7], presently at the 0.3% level, corresponding to about 60 μarcsec yr^{-1} [3]. Geodetic precession is primarily another measure of PPN γ. The Gravity Probe-B mission finalized a result on geodetic precession at the 0.28% level. Pulsar timing has thus far confirmed geodetic precession at the 13% level [57].

2.1.4. Inverse-square law, extra dimensions and other frontiers. Any deviation from the Newtonian $1/r^2$ force law produces a precession of orbital perigee. LLR's measurement of any anomalous precession rate of the lunar orbit limits the strength of Yukawa-like long-range forces with ranges comparable to the $\sim 10^8$ m scale of the lunar orbit to $<2\times10^{-11}$ times the strength of gravity [11]. This is the strongest available constraint on the inverse-square law at any length scale [12].

Measurement of the precession rate can also probe a recent idea (called DGP gravity) in which the accelerated expansion of the universe arises not from a non-zero cosmological constant but rather from a long-range modification of the gravitational coupling, brought about by higher-dimensional effects [18, 19, 58]. Even though the lunar orbit is far smaller than the Gigaparsec length-scale characteristic of the anomalous coupling, there would be a measurable signature of this new physics, manifesting itself as an anomalous precession rate at about 5 μarcsec yr^{-1}—roughly a factor of 10 below current LLR limits, and potentially reachable by millimeter-quality LLR.

Another example of new tests that LLR can perform is represented by the Standard Model Extension (SME), in which Lorentz-violating terms are introduced into the Standard Model of physics in order to generalize it [59]. Expressed in the gravitational sector [60], the SME exerts some influence on the lunar orbit [61]. Accordingly, LLR has been used to place constraints on the relevant SME parameters [62].

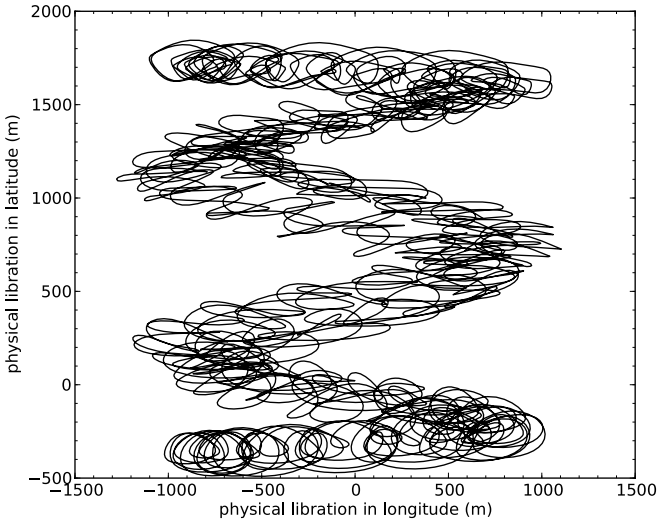

Figure 11. Physical librations of the Moon over 18.6 years, translated into displacement at the lunar surface. The main oscillation in longitude has a 1-year period, while the latitude exhibits a 6-year beat period between the lunar anomalistic month and the draconic month.

Offering a high-precision measurement of a clean dynamical system, LLR constitutes a comprehensive check on gravitational phenomenology. As such, we can expect that LLR will continue to exhibit sensitivity to future theories that challenge the foundation of GR.

2.2. *Lunar and Earth physics*

While tests of gravitation constitute a compelling suite of scientific motivations for pursuing LLR, details of the Earth and Moon also influence the range measurement, thereby opening lines of inquiry into the natures of these bodies. A more detailed treatment of these aspects appears in another review [3], and are here briefly summarized.

2.2.1. The Lunar interior. By virtue of the fact that the Moon's orientation, orbit, and tidal deformation are influenced by the interaction of its internal mass structure with torques and forces imposed upon it, LLR data can expose properties of the lunar interior otherwise unavailable.

The Moon is tidally locked to the Earth, with the equatorial bulge elongated in the Earth–Moon direction, resulting in a triaxial mass distribution—the associated moments of inertia labeled and ordered as $A < B < C$. Torques on this non-spherical body from the Earth, Sun, and larger/closer planets impose physical librations, or rocking, of approximately $\pm$120 arcsec in both longitude and latitude. This is distinct from the much larger 'optical' libration caused by Earth's changing vantage point of the Moon in its elliptical, inclined orbit. At the surface of the Moon, the physical librations translate into $\sim$1000 m amplitude motions (figure 11), allowing centimeter-level LLR to gauge the effect at the $\sim 10^{-5}$ level. Sensitivity to lunar physical librations has enabled determination of relative differences in the principal

moments of inertia, $\beta \equiv (C - A)/B$ and $\gamma \equiv (B - A)/C$ ($\sim 6.3 \times 10^{-4}$ and $\sim 2.3 \times 10^{-4}$, respectively), to the 0.05% level. In addition, the lunar quadrupole moment J_2 couples to the lunar orbit and is fit from LLR data. These three quantities together provide the best set of independent measurements by which to determine the principal moments of inertia. For instance, the polar moment, C, is found to be 0.393 ± 0.001 times MR^2, where a uniform density sphere would exhibit a numerical factor of exactly 0.4 [63]. The Earth, by contrast, is more centrally concentrated with a moment of inertia factor of 0.33.

If the Moon were a perfect fluid body, the tidal bulge caused by the Earth would have a peak-to-trough amplitude of 19 m. However, the Love number[2], h_2, for the Moon is very small, at about 0.04 (contrast to Earth $h_2 \approx 0.59$), so the total amplitude is held to less than a meter. Optical librations limit the motion of the bulge relative to the lunar surface to $\pm 8^\circ$, so that any given spot on the Moon sees tidal variations only at the level of $\sim$0.1 m, peaking at 45° from the Earth–Moon line. Varying distance between Earth and Moon contributes an additional ± 0.1 m deformation, aligned with the bulge [63].

The most sophisticated and successful lunar interior model resides at the Jet Propulsion Laboratory, for which the remainder of this paragraph applies. In addition to J_2, β and γ, any combination of third-order multipole coefficients may be fit from LLR data. Higher order terms and third-order terms that are not fit derive from Lunar Prospector data. In the numerical integration of lunar rotation, degree-2 Love numbers are considered, plus a time delay for lunar tides. Dissipation is represented by a term for friction at the core-mantle boundary and five out-of-phase periodic libration terms address the frequency-dependence of tidal dissipation. At the monthly tidal period, the dissipation is found to result in a rather low resonant quality factor, $Q \approx 33 \pm 4$. For extensive details on the dissipation model, and treatment of physical librations, see Williams *et al* [13], and Rambaux and Williams [64], respectively.

2.2.2. Earth orientation, precession and coordinate frames. Evaluating the center-to-center Earth–Moon range for access to gravitational physics relies on detailed knowledge of the three-dimensional orientation of the Earth at the time of observation. LLR can therefore contribute to our knowledge and understanding of the responsible phenomenologies. Earth orientation can be described as three Euler angles, broken into rotation about the polar axis, and two angles representing the direction of said axis on the sky. Additionally, the rotation axis migrates with respect to the geometrical surface on a 10 m scale over approximately annual periods (this includes the Chandler wobble[3]; see figure 12). The trajectory of the axis on the sky is largely deterministic, described by precession and

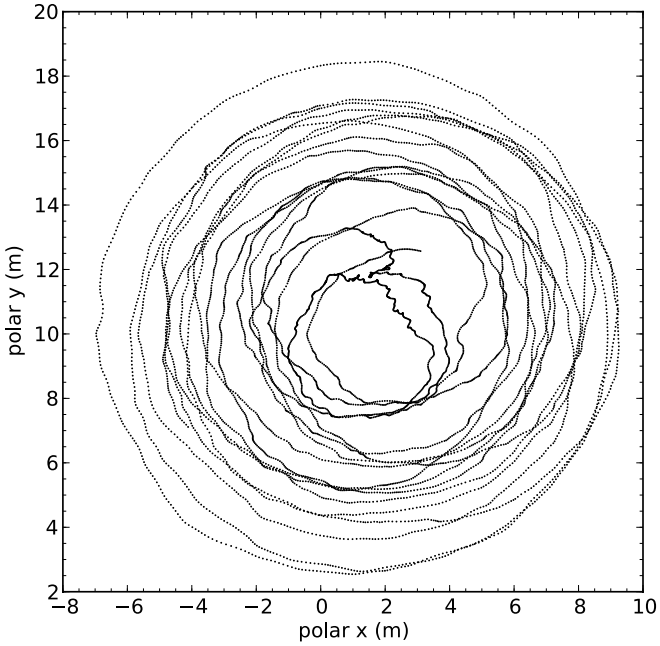

Figure 12. Migration of Earth's polar axis with respect to the body over 20 years, in one-day samples.

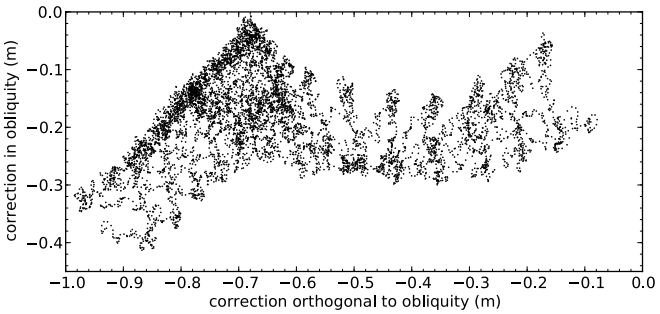

Figure 13. Empirical nutation corrections over 20 years, relative to the IAU1980 nutation theory, expressed in meters at the pole.

nutation[4] and related to known torques acting on the Earth's figure. Nutation is dominated by an 18.6-year term relating to precession of the lunar orbital plane, and amounting to the equivalent of 300 m at the Earth's surface. Earth's slowing rotation due to tidal dissipation (accompanied by an LLR-determined 3.8 cm yr^{-1} egress of the lunar orbit [65]) results in a secular phase offset in the rotation angle, also influenced by periodic phenomena like tides, and by aperiodic factors like angular momentum exchange between ocean, atmosphere, and land.

In practice, all five orientation parameters must be supplied or augmented by observational measurements or corrections. Nutation adjustments tend to be less than 1 m (figure 13). UT1, characterizing the rotational state relative to atomic time, can vary by as much as 3.5 ms in a day (accumulating to almost 1 s yr^{-1} around 1995), translating to 1.6 m at Earth's surface (figures 14 and 15).

[2] Love numbers describe the degree to which a body deforms relative to that of a perfect fluid body. Rigid bodies would have Love numbers near zero, while fluid bodies have Love numbers near unity. The primary Love numbers, h, l and k describe vertical displacement, horizontal displacement, and the degree to which the potential is modified by the redistribution of mass, respectively.

[3] The Chandler wobble is a free-mode (torque-free) nutation of the Earth's rotation axis due to Earth's non-axisymmetric mass distribution.

[4] Precession is the 26 000-year period migration of the Earth's polar axis with respect to inertial space, sweeping out a cone perpendicular to the ecliptic plane defined by Earth's orbit about the Sun. Nutation is the much faster wobble of the polar axis about the smooth precession trajectory due primarily to lunar and solar torques on the Earth's equatorial bulge.

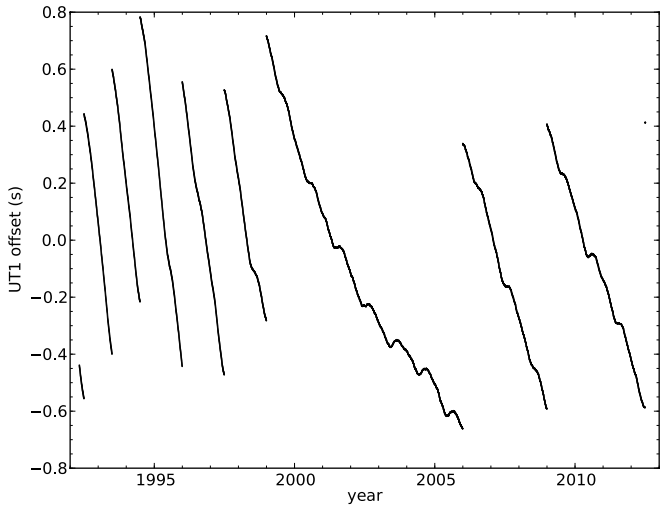

Figure 14. UT1, the offset from Coordinated Universal Time (UTC), over 20 years. Discontinuities reflect leap seconds. Annual wiggles can be seen in all tracks, but most clearly when the slope is smaller, as in the period from 2000–2005.

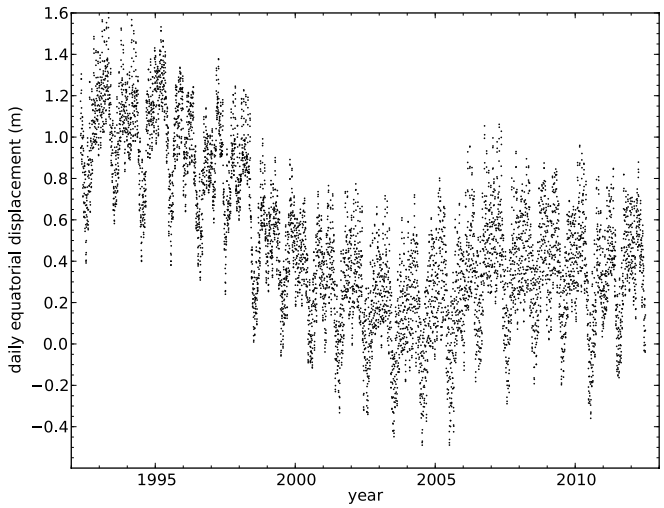

Figure 15. Length of day variations expressed as the displacement of the equator from one day to the next relative to a perfect 24-hour clock. The net positive bias is simply a consequence of Earth's slowing rotation due to tidal dissipation and is related to the 3.8 cm yr^{-1} egress of the lunar orbit. Large variations exist on top of this bias at a level that is important to LLR.

The point, again, is that LLR is sensitive to each of the Earth orientation parameters, so that the LLR dataset can be used to supplement our understanding of these phenomena (e.g. [66]). LLR data are therefore routinely combined with data from Very Long Baseline Interferometry (VLBI), GPS, satellite laser ranging (SLR), and Doppler Orbitography and Radiopositioning Integrated by Satellite (DORIS) in the Earth orientation parameters published by the International Earth Rotation and Reference System Service (IERS), who also periodically publish self-consistent, evolving methods for computing Earth orientation [67].

Finally, LLR also contributes to establishment of coordinate systems, especially in defining the relative orientation of the ecliptic and equatorial planes[5]. This in turn plays a role in establishing the celestial coordinate origin, whether in the International Celestial Reference System (ICRF) or the dynamical ecliptic/equator of J2000.0 (whose coordinate origins differ by 17 marcsec). Precession and nutation are defined with respect to the celestial frame, so that LLR's sensitivity to the Earth axis orientation ties into this context as well.

3. LLR capability across time

Beginning with a historical introduction, this section looks at past and current LLR capabilities, and how the current state of the art facilitates improved scientific return from LLR.

3.1. Brief LLR history

Less than two weeks after the landing of the first retroreflector array on the Apollo 11 mission, the first accurate laser ranges to the Moon were performed on 1969 August 1 from the 3.1 m telescope at the Lick Observatory. A few other sites around the world demonstrated lunar ranging capability around that time, but none of these stations—including the Lick Observatory—embarked on scientific campaigns to obtain meaningfully long time series of accurate ranges. However, one month after the Apollo 11 landing, a long-term effort using the 2.7 m telescope at the McDonald Observatory commenced ranging to the Moon [68], providing all of the scientifically relevant observations over the next decade. The McDonald station used a ruby laser with a 4 ns pulse width, firing at a repetition rate of about 0.3 Hz and ∼3 J per pulse. This station routinely achieved 20 cm range precision, with a photon return rate as high as 0.2 photons per pulse, or 0.06 photons per second. A typical 'normal point'—a representative measurement for a run typically lasting tens of minutes—was constructed from approximately 20 photon returns.

In the mid 1980s, a lunar ranging renaissance took place, with three capable stations beginning operation. In 1984, a French station at the Observatoire de la Côte d'Azur (OCA) [69] began collecting accurate ranges. Using a 1.5 m telescope, a 70 ps Nd : YAG laser firing at 10 Hz and 75 mJ per pulse, OCA became the premier lunar ranging station in the world and has contributed about half of the total range measurements to date. From 1984–1990, a station at Haleakala in Hawaii produced strong returns and accurate ranges. In 1985, the McDonald operation transitioned from the 2.7 m shared astronomical telescope to a dedicated 0.76 m telescope (also used for SLR) employing a 200 ps Nd : YAG laser operating at 10 Hz and 150 mJ per pulse. This station is referred to as the McDonald Laser Ranging System (MLRS) [70]. From 1990–2006, the MLRS and OCA stations were the only routine contributors to lunar range data with characteristic return rates of 0.002 and 0.01 photons per pulse, respectively. Normal points from the two stations typically consist of 15 and 40 photons, respectively. More complete histories of these and other efforts

[5] The ecliptic plane is the plane of the Earth's orbit about the Sun. The equatorial plane is a projection of the Earth's equator into inertial space.

(Russia, Pic du Midi, Australia, Japan, etc) may be found in other works [20, 22, 68].

Presently, five stations in the world exhibit LLR capability: OCA, MLRS, Apache Point, Matera, and Wetzell—although only the first three acquire data regularly. After a shutdown from 2005–2010, OCA is back in regular operation, although at about half its former pace. Since 2007, the Apache Point Observatory Lunar Laser-ranging Operation (APOLLO; for which the author is the principal investigator) has led the LLR data effort both in terms of number of normal points and estimated range uncertainty. Averaging about 260 measurements per year and a median statistical uncertainty per normal point of less than 3 mm, APOLLO seeks to effect a substantial improvement in LLR tests of gravity.

3.2. APOLLO apparatus and performance

This section provides a brief overview of the APOLLO apparatus and its demonstrated performance. A full description of the apparatus can be found in [71]. APOLLO employs a laser averaging 2.3 W at 532 nm, generating 100 ps pulses at a 20 Hz repetition rate and 115 mJ per pulse. The laser is transmitted from the 3.5 m aperture telescope at the Apache Point Observatory in southern New Mexico at an elevation of 2.8 km. The full aperture is utilized for beam transmission. A small portion of the outgoing beam is intercepted by a corner cube reflector prism attached to the telescope secondary mirror, sending light back to the receiver, attenuated to the single-photon level and providing a precise measure of the pulse departure time. The receiver houses a 4×4 avalanche photodiode (APD) array capable of high-precision timing of single photons at a detection sensitivity around 30%. The array occupies a re-imaged focal plane of the telescope, spanning 1.4 arcsec on a side. This arrangement results in an oversampled point spread function, while providing spatial information useful for tracking feedback. Photon arrivals create START pulses for a 16-channel time-to-digital converter (TDC) with 15 ps jitter and 25 ps bins. STOP pulses to the TDC are extracted from a 50 MHz low-phase-noise clock pulse train, and the number of clock pulses between the STOP signal for the local corner cube return and the STOP signal for the lunar return is counted. The master clock on which the 50 MHz pulse train is generated uses an ovenized quartz crystal disciplined by reference to GPS so that the 2.5 s round-trip travel time is measured against a reliable frequency standard, and the absolute time is known far better than the microsecond level required for millimeter range precision. Table 1 reproduces the contributions to APOLLO's random uncertainty from the instrument description paper [71].

The large telescope aperture, good atmospheric seeing, and array detector together result in high-signal rates and allow confident signal optimization through pointing corrections and velocity aberration compensation—controlled by affecting a deliberate offset in transmitter and receiver pointing directions. Consequently, APOLLO signal rates exceed those of previous stations by a substantial margin. Table 2 displays APOLLO's record performance on each reflector. Since each entry is associated with 5000-shot data runs, each transpired over approximately 250 s, at a 20 Hz pulse repetition rate. The 'photons' column corresponds to detected photo-electrons, sometimes exceeding one photon per shot, as enabled by APOLLO's multi-element APD detector. The "rate factor" compares APOLLO's peak photon rate (photons/minute) to that of the previous LLR record for each reflector, held in every case by OCA—except for Lunokhod 1, which was first recovered by APOLLO, as described in section 4.1.

Table 1. APOLLO random error budget per photon.

Error source	RMS error (ps)	RMS error (mm)
APD illumination	60	9
APD intrinsic	<50	<7.5
Laser pulse	45	7
Timing electronics	20	3
GPS clock	7	1
Total APOLLO	93	14
Retroreflector array	100–300	15–45
Total random uncertainty	136–314	20–47

Table 2. APOLLO record rates.

Reflector	Shots	Photons	Photons/ shot	Photons/ minute	Rate factor
Apollo 11	5000	4784	0.96	1148	69
Apollo 14	5000	7606	1.52	1825	69
Apollo 15	5000	15730	3.15	3775	67
Lunokhod 1	5000	2070	0.41	497	—
Lunokhod 2	5000	1301	0.26	312	54

Greater photon count is not in itself indicative of higher precision range measurements. But to the extent that the temporal spread of the lunar return is dominated by the finite size of the reflector array—tilted by lunar libration—high photon number is a necessary ingredient in reducing statistical uncertainty, as was illustrated in section 1.3. Two different evaluations of APOLLO's millimeter-level performance have been published elsewhere [72, 73].

3.3. APOLLO advantages translated to science

The aforementioned signal optimization capability of APOLLO naturally translates into faster acquisition and a higher signal rate (see figure 8 for an example), which enhance the range precision and scientific usefulness of the data. But a number of derivative advantages emerge as well, outlined here. As a general statement, systematic effects are more easily exposed in a high-signal regime.

Foremost, APOLLO routinely ranges to four, and sometimes five reflectors in each observing session. Typically, it is possible to make several circuits of the reflectors within the ∼1 hr time allocation (figures 16 and 17). The result is that lunar orientation and deformation are well-established during each session. This bestows an obvious advantage onto understanding of the lunar interior, but also enhances the ability to represent accurately the location and trajectory of the center of mass of the Moon—important for testing gravitation.

Having multiple detector channels essentially provides many independent measurements: each channel receives

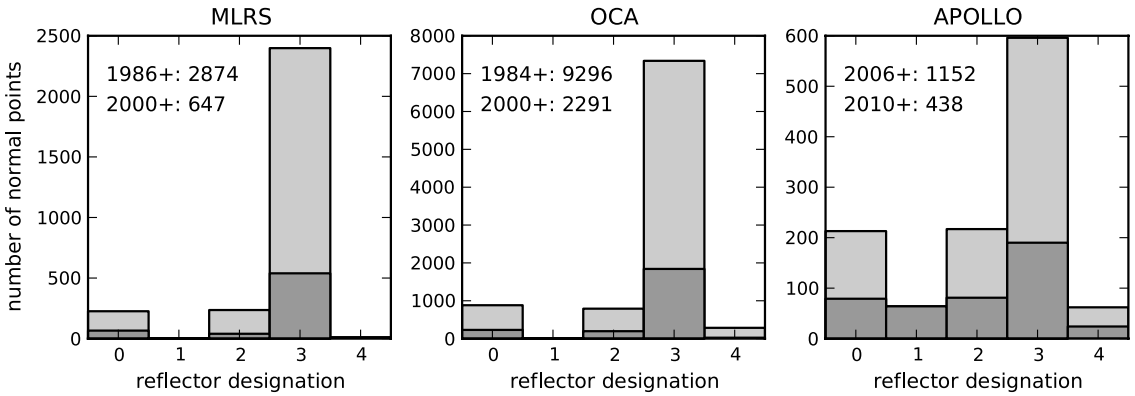

Figure 16. Distribution of normal points among the five reflectors for the chief modern LLR stations. Reflectors are numbered in order of arrival from 0–4, corresponding to Apollo 11, Lunokhod 1, Apollo 14, Apollo 15 and Lunokhod 2. Overlaid on each is a darker histogram representing more recent data, the break point being 2000.0 for the longer-lived stations and 2010.0 for the newer APOLLO. Apollo 15 dominates for all stations, being a larger, more easily acquired target.

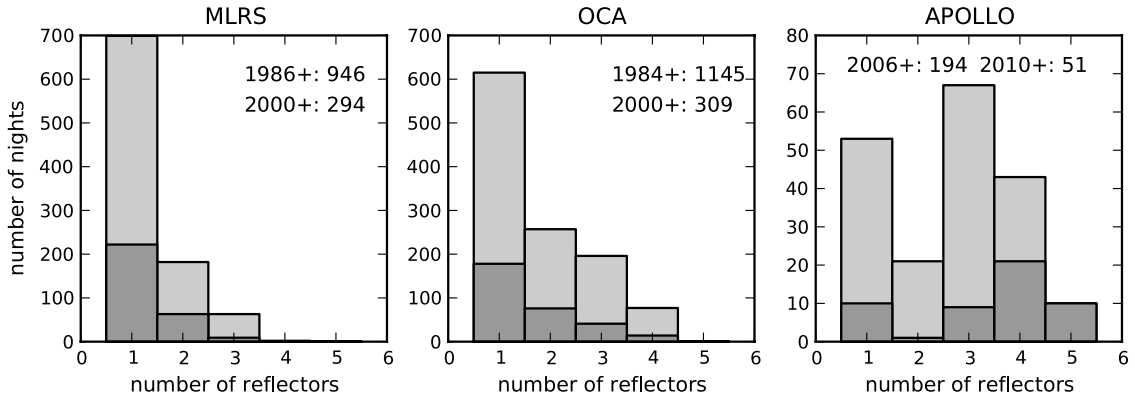

Figure 17. Number of reflectors acquired per night of observation for the chief modern LLR stations. Shading follows the convention of figure 16. The mode for the older stations has been one reflector per night (both overall, and recently), whereas APOLLO's nominal mode has been three reflectors, recently moving to four.

photons from the local (fiducial) corner cube as well as from the lunar array. One may then compare 'answers' from each of the channels to get a separate handle on measurement error. The degree to which measurements disagree provides a check on estimated uncertainties.

The signal rate is high enough to permit exploration of the physical orientation of the reflector arrays on the Moon via evolution of the temporal response as a function of lunar libration. This is especially effective on the larger, rectangular Apollo 15 array, which appears to have a 2° azimuth offset, but otherwise nominal tilts. The smaller Apollo arrays are consistent with nominal pointing, although probed less accurately. Incorporating array orientation information into the data reduction routines allows a higher fidelity fit to the observations, reducing the opportunity for systematic offsets. Ultimately, it may be possible to elucidate spatial variability of response across the reflector array.

4. Recent surprises

The recently increased LLR return rate has facilitated some new findings, two of which are detailed here: first the re-discovery of a reflector that had been lost for nearly four decades; followed by an account of evidence for degraded reflector performance.

4.1. Finding Lunokhod 1

Starting in 2008, APOLLO devoted some observing time to searching for the lost Lunokhod 1 reflector. Accurate coordinates were not available, so searches were referenced to the best-guess coordinates of the time [74]. Given a ∼2 km beam footprint, the 5 km positional uncertainty can be scanned in a matter of minutes, so that angular parameter space was not the main limitation. Rather, the 100 ns timing gate used for the APD detector array translates into a ±7.5 m line-of-sight uncertainty, intersecting the tilted lunar surface at the position of Lunokhod 1 in a ∼20 m swath. Therefore searches concentrated exclusively on the temporal domain while pointing at the nominal position and allowing natural pointing excursions to provide some degree of angular coverage.

The Lunar Reconnaissance Orbiter (LRO) helped in three ways. Most indirectly, corner cube prisms were placed on LRO in the hope that APOLLO could obtain two-way range measurements to the spacecraft. This prompted APOLLO to develop a wide-gate (800 ns) mode to cope with positional

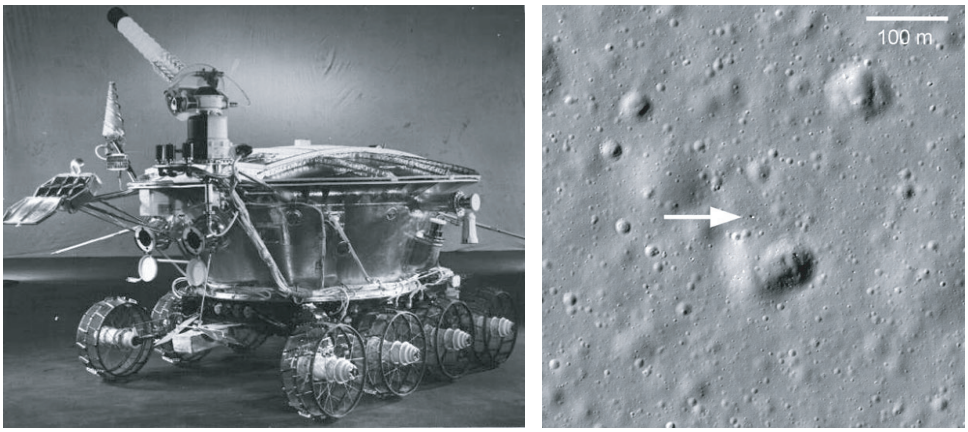

Figure 18. Two Lunokhod rovers, one of which is pictured at left, were landed and operated on the lunar surface, both possessing a retroreflector array (visible as a tilted tray protruding from the rover body at far left; image courtesy the Lavochkin Association). Any records of successful ranging to the first rover were lost to the international community, so that accurate coordinates were unknown, and nearly 40 years passed without range measurements. In 2010 March, NASA's Lunar Reconnaissance Orbiter Camera (LROC) obtained the image at right, locating the rover (arrowed) to approximately 100 m accuracy. Successful ranging has thenceforth been possible, the reflector appearing to be in better health than its twin on the Lunokhod 2 rover.

uncertainty of LRO. Second, LRO's Lunar Orbiter Laser Altimeter (LOLA) provided an accurate radial coordinate of the plain on which Lunokhod 1 sits. But by far the most important contribution was high-resolution imaging, identifying the rover in 2010 March, and providing coordinates accurate to approximately 100 m (figure 18).

On 22 April 2010, APOLLO got a strong return from the Lunokhod 1 reflector, appearing 270 ns later than the time prediction based on the LRO-provided coordinates. Recording about 2000 photons in the initial 10 000 shot run, Lunokhod 1 had instantly outperformed the best photon yield APOLLO had seen over 5 years of observing the Lunokhod 2 reflector (in 44 prior measurements). Since this time, the position—displaced from the earlier working estimate by 5 km, and off from the LRO-provided coordinates by 100 m—has been refined to the centimeter level [75].

The Lunokhod 1 reflector is located 50° from the selenographic coordinate origin, making it the farthest reflector from the apparent lunar center: about twice as far as the Apollo reflectors (figure 3). This makes Lunokhod 1 a more sensitive probe of lunar orientation than the other reflectors. Moreover, its location allows sensitivity to librations in both latitude and longitude, while the Apollo reflectors lie close to the equator or prime meridian, resulting in each being mostly sensitive to librations in only one principal dimension.

4.2. Reflector degradation

Despite confident optimization of telescope pointing, velocity aberration correction, laser beam divergence, and telescope focus (see section 3.2), the APOLLO link budget has never matched its carefully calculated theoretical potential—falling short by an order of magnitude, even on the best nights [76]. This appears to be true for other LLR stations as well, based on comparing performance to expectations with respect to system parameters. More telling is the observation that the signal level near full-moon phase drops by another order of magnitude [23]. Examination of the earliest range data from the McDonald 2.7 m telescope reveals the slow onset of this phenomenon, so that the cause appears to be progressive in nature.

Lunar eclipse observations contribute a substantial clue, in that the signal performance soars to normal levels within 15 min of entering full shadow. This strongly suggests solar energy absorption leading to thermal gradients in the corner cube prisms. The Apollo corner cubes and associated mounts were carefully designed to minimize solar absorption and thermal gradients by a combination of total internal reflection, recessed corner cubes, radiation-resistant substrate, and minimization of mount conductance. Thermal simulations predicted a central irradiance of the far-field diffraction pattern emerging from the corner cubes at full moon to be >90% of the peak performance. A gradient as small as ∼4 K from the front surface to the corner cube vertex essentially nullifies the central irradiance [77].

The most likely explanation is the slow accumulation of a very thin layer of dust on the reflector front surface, transported by electrostatic levitation (via photoionization and solar wind charge deposition [78, 79]) and cascading disturbances from impacts. Approximately half of the reflector surface would need to be covered by dust to produce a ten-fold reduction in central irradiance, since each dust grain counts twice in a double-pass of the front surface, and the central intensity otherwise scales as the square of the clear area. Meanwhile, this same ∼50% fill-factor could result in enough front-surface energy absorption to generate a thermal gradient sufficiently large to cause an additional large signal deficit.

Indeed, the eclipse observations validate this picture, in that after the initial signal surge upon entering shadow, the return strength plummets to sub-detectable levels. When light returns, the signal peaks again before settling back to levels typical for the full moon. The interpretation is that initially the corner cube has a strong positive thermal gradient owing to a heated front surface. As the solar illumination fades, the corner cube begins to radiate its stored energy to space via the front surface, cooling off and reversing the gradient. A zero-crossing occurs as the gradient evolves from positive to negative, so

that the reflector performance momentarily recovers during the approximately isothermal state. When light returns, the gradient changes sign again, passing through zero a second time for a temporary surge in signal strength.

One final aspect of the degradation story is that Lunokhod 2 was initially observed in 1971 to be comparable in strength to the Apollo 15 reflector. Indeed, cross section predictions put the expected Lunokhod response midway between the 100-element Apollo 11/14 reflectors and the 300-element Apollo 15 reflector. Today, Lunokhod 2 registers at about 10% the strength of the Apollo 15 array. Thus it is clear that the reflectors can experience *relative* changes in performance over time. Meanwhile, the three Apollo reflectors are observed to maintain a 3:1:1 ratio, and all exhibit a comparable full-moon deficit. The Lunokhod 1 array typically performs similarly to—if not better than—the smaller Apollo arrays. Its degradation therefore appears to be roughly in step with that of the Apollo reflectors, making the identically designed Lunokhod 2 reflector the truly anomalous case.

The possibility of dynamic dust on the Moon impacts ambitions for lunar-based telescopes or mechanical equipment. The still-functioning reflectors have often been held up as evidence that dust is not a major issue. The recent observations described here cast doubt on this picture.

5. The modeling challenge

Sitting between accurate range measurements and scientific results is a complex model whose development must keep pace with observational advances in order to realize the full potential of LLR. Here we describe the requisite components of a model, discuss current capabilities, and explore improvements to be made.

5.1. Model content/construction

The crux of any scientific endeavor is the comparison between theory and experiment. For LLR, the theory piece is represented by a model of the solar system incorporating some prescription for gravity and all other physical effects that can render an impact on the measurement. For example, Venus and Jupiter generate perturbations in the Earth–Moon separation on the order of 1 km, Mars and Saturn at the 100 m level, and even the largest asteroids chalk up millimeter-scale deviations. It is therefore clearly important to have an accurate representation of solar system dynamics.

But because LLR is performed in relation to the *surfaces* of the Earth and Moon, it is also necessary to provide accurate descriptions of body orientations and deformations. In the case of the Earth, non-deterministic mass flows in the atmosphere and ocean complicate matters. Body torques between Earth and Moon not only affect orientation, but also couple into orbital dynamics. Tidal dissipation likewise translates into an orbital egress of the Moon at the rate of about 38 mm yr^{-1}. Crustal loading influences from the ocean, atmosphere, and ground water come into play for the Earth station.

Light propagation effects must also be considered. Sensibly cast in the SSB frame (see section 1.4), the light path forms two legs of a generally asymmetric triangle. The Shapiro delay associated with propagation through solar and terrestrial gravitational potentials must be incorporated, amounting to a $\sim$25 ns modification to the round-trip time (3.7 m one-way equivalent due to the Sun; 0.02 m from the Earth potential). Propagation through the atmosphere incurs a roughly 2 m path delay that must be determined and removed to high precision.

The model itself is constructed as a parameterized physical description, many pieces of which are numerically integrated simultaneously. For example, solar system bodies are represented as point masses, where model parameters are initial positions and velocities, and the associated mass values. The Earth and Moon and Sun are treated as non-point masses, in which case the dynamical torques are jointly computed to follow the dynamical evolution of the system. Partial derivatives of the computed range with respect to each model parameter are calculated for each measurement epoch so that a least-squares covariant parameter adjustment may be executed. By iterating such adjustments, the set of LLR observations can be used to converge on a physical description of the solar system that is optimally consistent with the data. A cute way to put this is that millimeter-level measurement/model fidelity in the Earth–Moon range can in principle determine the mass and position of Jupiter to a part in a million, given the kilometer-scale influence Jupiter has on the lunar orbit. In practice, irregular data sampling together with correlations between many model parameters compromise complete separation of variables. Over the long term, periodic effects from solar system bodies tend to be separable. But some parameters tend to remain highly correlated, like the GM value for the Earth–Moon system and the semi-major axis of the lunar orbit. A diverse set of other solar system observations complement LLR data to optimally determine solar system model parameters.

5.2. Current capabilities

Several LLR models exist in the world, sited at the Jet Propulsion Laboratory (JPL), the Harvard-Smithsonian Center for Astrophysics (CfA), the Leibniz University in Hannover, Germany, and at the IMCCE in Paris, France. Of these, only the Planetary Ephemeris Program (PEP), at the CfA, is made available to the community (and as open-source code). The JPL model currently demonstrates the best performance, producing weighted RMS residuals for both APOLLO and OCA data in the neighborhood of 18 mm, which is roughly a factor of two better than the other models at present. Clearly a gap exists between estimated APOLLO uncertainties of a few millimeters and the model residuals.

The CfA, Paris and Hannover efforts are currently engaged in a stepwise comparative effort to identify model differences, shortcomings, and errors. Additionally, APOLLO data are being used to illuminate one aspect of model performance by exploiting the fact that most observing sessions result in measurements to multiple reflectors. This provides a nearly direct measurement of lunar orientation, the robustness of which is confirmed on occasions when several circuits of the reflectors are made in a short period [73]. In brief, the result of this exercise is a determination of how much adjustment is

Table 3. Libration adjustment weighted RMS in nanoradians.

Model	Longitude adjustment (nrad)	Latitude adjustment (nrad)
JPL	5.1	7.3
CfA	19	23
Hannover	23	36
Paris	29	76

needed in the latitude and longitude librations of the Moon to bring the residuals among the reflectors in line with each other. The results are summarized in table 3. For reference, 1 nrad of angle translates to 1.7 mm of range at the lunar limb, or about 0.7 mm at the typical position of an Apollo reflector. Again it is clear that JPL has an advantage over the other efforts, although the Paris result does not represent a least-squares-adjusted integration, but rather uses the JPL exported ephemeris, DE423.

Lunar orientation is one of many components in the model, so that adjusting the librations in an *ad hoc* manner based on APOLLO residuals does not markedly improve the overall RMS of residuals—the main effect being to better cluster residuals from different reflectors within each night. Night-to-night variations still dominate, and tend to look wholly different from one model to the next.

5.3. Charted improvements

Each LLR analysis group has its own list of known effects yet to be incorporated into the model—many of which are only beginning to be important at the millimeter level. By way of example, the following is a list of known effects not yet incorporated into PEP at CfA. Other groups may be in different states with regard to these items. For PEP, specific improvements to be made include:

- a more complete treatment of dissipation in the lunar interior, following JPL's lead;
- a more rigorous tidal model, applying Love numbers that depend on frequency and spherical harmonic degree and order, aided by inputs from VLBI and GPS;
- updating the gravitational multipoles of the Earth and Moon, using the latest data from the GRACE and GRAIL missions, respectively;
- improved Earth orientation handling, including feedback of LLR residuals into the VLBI/GPS-determined data;
- ocean loading, having approximately 3 mm horizontal RMS and 5 mm vertical RMS at the APOLLO site, for instance;
- atmospheric loading, having an impact of roughly 1 mm for every 3 mbar of pressure anomaly;
- earth center-of-mass motion, seen via SLR to have a ∼1 cm amplitude at an annual frequency.

Addressing the first three items—together with any errors discovered in the model intercomparison between PEP and the European models—may in fact bring PEP in line with the present JPL model capability. The remaining effects could conceivably add up to accommodate the ∼2 cm residuals still exhibited by the JPL model. We discuss them here.

Table 4. Ocean loading amplitudes at apache point.

Component	RMS (mm)	Minimum (mm)	Maximum (mm)
North–South	2.26	−5.88	5.57
East–West	1.57	−3.52	4.51
Vertical	5.46	−14.71	11.91

Sophisticated models exist for tidal ocean loading that describe site motion at the sub-millimeter level—easily so for APOLLO, since the semi-diurnal load tides at Apache Point happen to be small. Table 4 presents modeled site displacements from ocean tidal loading at the Apache Point site by the TPXO 7.0 model. Other models (GOT00 and CSR4) produce results consistent to within about 0.5 mm.

For the various sources of non-tidal loading, the best results will come from a combination of the global pressure fields produced by the various branches of the Global Geophysical Fluids Center [80]: air pressure, ocean mass, and ground and surface water. Global models for these are advancing rapidly thanks to data from the GRACE mission [81, 82]. These can be improved by combining, for example, global models of air pressure with the more detailed ("mesoscale") local models that are now produced for regional weather forecasting.

SLR measurements show a displacement of Earth's center-of-mass with respect to coordinates of the geometrical center (as defined by a network of ground stations). This motion has a roughly annual period and an amplitude of about a centimeter [83–85]. LLR analysis has not yet incorporated this effect. However, the presence of the nearby a GPS station (described in section 5.4) will allow us to incorporate the SLR result on geocenter motion into the analysis of APOLLO data.

Additionally, radiation pressure is known to be a 3.65 ± 0.08 mm $\cos D$ effect that can be applied [86]. Likewise, atmospheric propagation delay, a ∼2 m effect, has been recently modeled to sub-millimeter accuracy for elevation angles above 20° [87, 88], and has since been incorporated into PEP.

5.4. Uncharted improvements

As described, the items in the previous section are moderately well understood, in most cases having mature models and complementary observations providing input. But millimeter-quality LLR data will likely strain current models and demand that new physical effects be addressed.

APOLLO is provisioned to check how well displacements are being modeled by comparison to supplemental measurements of:

- site position by a nearby GPS station (P027 in the Plate Boundary Observatory network; 2.5 km away); and
- local g by a superconducting gravimeter (SG) at Apache Point.

For daily averages of the GPS positions at the P027 site typically have uncertainties of about 1.5 mm horizontally, and 6 mm vertically. Monthly averages—where LLR signatures are most relevant—have 0.3 mm horizontal and 1.2 mm vertical uncertainties. Systematic errors prevent these precisions from

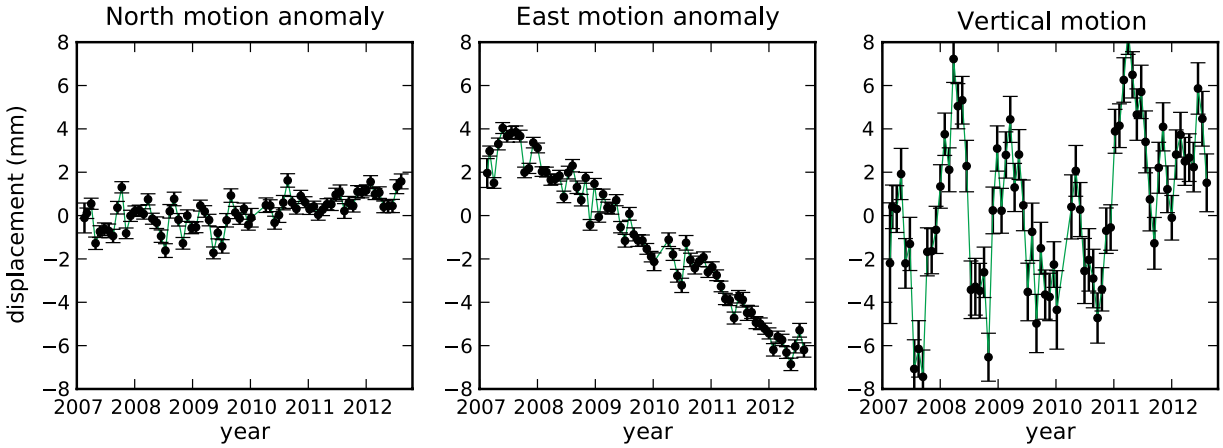

Figure 19. GPS data from the P027 Plate Boundary Observatory station located 2.5 km away from the Apache Point Observatory (on a similar summit). Data are binned in lunar-monthly units. Motions are shown *relative to* the North American plate, moving at (−6.3, −11.5, −0.6) mm yr^{-1} in the north, east, and up directions. The net motion of station P027 with respect to the global frame becomes (−6.05, −13.35, +0.2) mm yr^{-1}. The vertical motion indicates peak-to-peak site displacements exceeding 1 cm, highlighting the need to incorporate geodetic measurements into millimeter-quality LLR analysis.

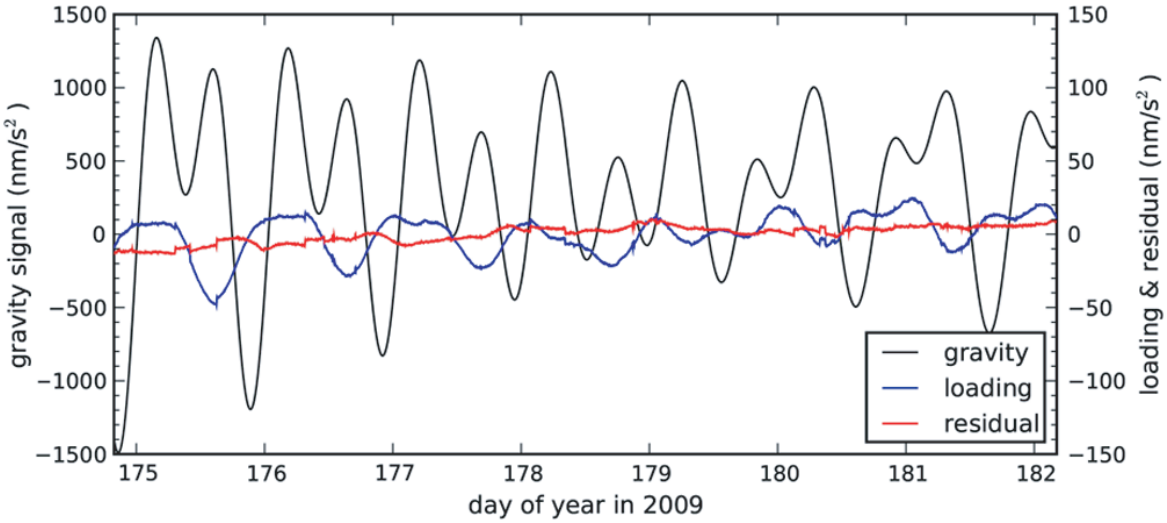

Figure 20. One week of SG data at Apache Point. The harmonic (black) line is not a model, but raw SG data filtered to 1 min samples. The semi-periodic (blue) line—referenced to the right-hand scale at 10× magnification—is the residual after subtracting a tidal model and local atmospheric influence, but not ocean or hydrologic loading signals. The flatter (red) curve is after removing ocean loads. Steps/jumps visible in the red line are attributed to rotations of the gravitationally asymmetric telescope dome, which can be subtracted using a record of dome motion. A gravity deviation of 1 nm s^{-2} corresponds to 0.18 mm of displacement for tides, and 0.3 mm for ocean loading, meaning that the peak-to-peak motion represented here amounts to more than 0.5 m.

direct translation into accuracies for motions relative to the Earth's center of mass, but the GPS data can still usefully check models for site displacements. Figure 19 shows data from the P027 site over 4 years, binned into periods of 27.55 days (monthly periods are especially relevant to LLR science). In the future, local GPS measurements may be used to constrain site displacements in a simultaneous fit to LLR data.

Likewise, precision gravimetry can complement the vertically challenged GPS measurements by monitoring surface gravity variations. A superconducting gravimeter mounted on the telescope pier of the Apache Point 3.5 m telescope has the sensitivity on 1 min timescales to resolve 0.1 mm vertical displacements by virtue of the fact that surface gravity diminishes by 3 nm s^{-2} for every millimeter of motion away from the center of the Earth.

The SG data measure local gravity variations with very low noise, excellent calibration stability, and low instrument drift. When the 1 Hz sampled data are filtered to remove microseisms (typically 20 nm s^{-2} peak-to-peak; 5–15 s periods), the short-term noise level is less than 0.3 nm s^{-2} peak-to-peak, corresponding to 0.1 mm in vertical displacement. Figure 20 shows tides dominating the SG signal, but removal of tides and local atmospheric influence leaves a 60 nm s^{-2} peak-to-peak signal dominated by ocean loading, which when removed reveals small signals such as the gravitational influence of the rotating telescope dome.

But a measurement of surface gravity only serves as a *proxy* to displacement. Direct gravitational attraction of loading sources (atmosphere, ground water) complicate the picture, and the mass redistribution accompanying

tidal displacements change the potential—and therefore the gradient of the potential, which is the measured quantity. For tidal displacements, knowledge of the Love numbers[2], h and k, and the deforming potential, W, allows conversion from a measurement of the variation in gravitational acceleration, Δg, to a vertical displacement, Δz, via $\Delta g = -(1 + h - \frac{3}{2}k)\frac{\partial W}{\partial r}$, and $\Delta z = (1+k-h)W/g$. In principle, knowledge of the Love numbers could come from the SG and/or the LLR fit. A better source may be the recently much-improved elastic models for the Western US resulting from the USA Array seismometer project. But some uncertainty remains in extrapolating from seismic frequencies to periods around a month.

A modeling challenge of the future may be to apply the tidal model to simultaneously fit the LLR data and gravimetry data. A demonstrated ability to model the SG data—especially the long-period terms—will provide an important estimate of the uncertainty from loading that can be included in fits to the data. Part of the SG campaign involves occasional comparison to a visiting absolute gravimeter in order to calibrate long-term drift in the SG instrument.

In a similar vein, while atmospheric propagation delay is well described by measuring pressure, temperature, and humidity at the observing site and applying a mapping function to the elevation of the observation [87, 88], horizontal pressure gradients may foil the usual single-point pressure measurements. Using regional pressure data (also useful for atmospheric loading corrections) has been demonstrated to improve results [89]. If greater precision is required, incorporation of data from a kilometer-scale barometric array may be employed to probe pressure gradients near the observatory—which may be impacted by wind interacting with geographical features, leading to dynamic pressure effects in the vicinity.

5.5. Periodicity and data span

In this section, we look at temporal aspects of the LLR measurement and its related science goals. In the face of the large list of phenomenological influences on the fundamental LLR measurement outlined in the preceding sections, it is important to remember that most of the science goals outlined in section 2 rely on *periodic* range signatures. Clearly the EP signal is periodic, displaying a cos D form at a period of 29.530 589 days. This is likewise true for gravitomagnetism and certain preferred-frame effects. But even secular effects ultimately derive from periodic observables. For instance, a variation in G alters the Keplerian relationship between period and semi-major axis. The resulting secular change in period results in a quadratic phase evolution. Obviously LLR provides a nearly direct measurement of the semi-major axis, but it is also directly sensitive to the phase of the 21 000 km amplitude periodic variation due to orbital eccentricity. Likewise, sensitivity to precession of the orbit is provided by monitoring the phases of the large-amplitude periodic behaviors in the orbit.

The key point is that largely aperiodic phenomena like atmospheric loading, variations in atmospheric propagation delay, or anomalous meanderings in Earth orientation are unlikely to mimic science signals at key lunar orbit periodicities. Obviously, greater sensitivity to interesting science signals will derive from doing the best possible job modeling confounding influences, effectively lowering the background against which to seek small anomalous periodic signatures.

Even with this in mind, in order to take full scientific advantage of the remarkable precision offered by LLR, the data must extend over a long enough span to sample long-period terms in the lunar orbit so that secular/aperiodic trends can be distinguished from periodic signatures and optimum amplitudes of the various periodic signatures can be obtained. This generally requires a data span of at least a half-period—and preferably longer—of the longest important periodic term. The various monthly periods: draconic[6] (nodal passage: 27.212 208 days); sidereal[7] (inertial space period: 27.321 661 days); and anomalistic[8] (perigee-to-perigee: 27.554 551 days) combine to give periods of 6.00 years, 8.85 years and 18.6 years. While the complete LLR record now spans two of these longest periods, not all of these data are of comparable precision. There is also a 75 yr wobble in the physical libration with a ∼70 m amplitude [64].

How might we expect formal uncertainties to scale with data span? For the periodic signals associated with the EP, gravitomagnetism, and preferred-frame effects, the uncertainty should scale as $T^{-0.5}$ if the sampling is approximately uniform in time, where T is the data span. For secular drift of the lunar orbital phase due to geodetic precession, deviations from the inverse-square law, or extra-dimension-motivated precession effects, sensitivity scales as $T^{-1.5}$, where the additional power of T comes from a longer baseline. For $\dot{G}$, which effectively gauges secular change of the orbital radius against that of the orbital period, the uncertainty scales as $T^{-2.5}$, where two powers of T come from the aforementioned quadratic evolution of phase. These scalings only apply to the extent that modeling capabilities are able to take full advantage of the measurement precision.

6. Future advances

We discuss here potential future directions for LLR, together with a qualitative assessment of resulting scientific gains.

LLR has for decades stayed at the forefront of tests of gravity, probes of the lunar interior, and determination of Earth coordinate systems. Recent improvements to the technique have stimulated a push to improve modeling capabilities, which are expected to produce further gains in the short term. Additionally, the LLR enterprise has largely been confined to the northern hemisphere. Steady data flow from a southern hemisphere station would allow better coverage of low-declination observations and better constrain Earth orientation.

[6] The draconic month describes the mean time between the Moon's consecutive crossings of the ecliptic plane in the ascending direction.

[7] The sidereal month is the mean time it takes for the Moon to return to the same direction in inertial space relative to the Earth center.

[8] The anomalistic month refers to the lunar mean anomaly, or phase/angle with respect to perigee.

6.1. Next-generation reflectors

Longer-term, improvements at the lunar end offer the biggest advantage—in the form of either new reflectors, an active transponder, or both. The current reflectors limit performance in a compounded way. Most fundamentally, the finite extent of the reflector array spreads the temporal width of the pulse by virtue of the fact that the array normal tilts away from the line of sight by up to 10° due to lunar libration (figures 5 and 6). This spread can be as large as one nanosecond for the Apollo 15 array at full-tilt, corresponding to a RMS measurement uncertainty approaching 50 mm (330 ps; see figure 7). Statistical centroiding of the signal to millimeter-level range precision requires hundreds or thousands of photons. This is how APOLLO reaches the millimeter domain, but such an approach is not feasible for other LLR stations. Degraded reflector performance (section 4.2) only exacerbates this problem. Thus the brute force approach to LLR by gathering more photons becomes more challenging with time.

Meanwhile, the spread imposed by the tilted reflector array eliminates incentives to improve ground-based laser pulse width or timing systems in any incremental fashion, since these errors add in quadrature to the dominant reflector spread. Improving APOLLO's 100 ps laser pulse width and 20 ps timing system—even by a factor of two—would have little discernible impact on the net timing precision, and so would appear to be wasted effort. Installing a larger array on the Moon also has no effect, as doubling the linear dimension doubles the temporal spread, requiring four times the signal for statistical reduction to the same level—which is exactly what a double-sized array delivers: no precision gain.

Simply making a sparse array of corner cubes so that each one could easily be resolved by ∼100 ps laser pulses would break the logjam. Improvements in ground systems would then have immediate impact. Halving the laser pulse width would consequently require four times fewer photons for similar statistical precision. Most locations on the front face of the Moon see the Earth permanently well away from local zenith, so that a modest lateral separation on the ground (>10 cm) is sufficient to separate the returns unambiguously.

A few current efforts are underway to explore next-generation reflectors for the lunar surface. Hollow corner cubes are being explored at the Goddard Space Flight Center using an ultra-stable quartz bonding technique [90]. Somewhat further along, work on 100 mm diameter fused silica corner cubes is in the space-environment testing phase to verify mitigation of thermal gradients in the presence of solar illumination [91].

6.2. Transponders

Installing active laser transponders on the lunar surface would have perhaps an even greater impact on LLR science. Replacing the $1/r^4$ signal loss regime with a far more benign $1/r^2$ regime would allow the extensive SLR network to engage in LLR on a routine basis. This would have tremendous impact in data volume, global distribution (fixing the southern hemisphere deficit, for instance), tie-in to well-established geodetic stations, and improvements in Earth surface/atmospheric models by using the Moon as a reference object largely unaffected by non-gravitational forces—unlike satellites. In this context, transponders work best in asynchronous mode, rather than echoing detected incoming signals. This permits the transponder to transmit a steady pulse train tied to a good clock while recording times of incoming signals with respect to this clock. The asynchronous mode has much greater noise immunity and thermal stability than echo-based techniques. Such transponders also pave the way for interplanetary laser ranging. The scientific benefits and hardware requirements for one such system has been explored in the context of laser ranging to Phobos [92].

6.3. Impact on science

On its face, improvement of LLR measurement precision as facilitated by new reflectors, transponders, and concomitant ground station upgrades has the potential to sharpen our constraints on (or find deviations in) gravitational physics by a corresponding (equal) factor. Time scales for improvement vary for different science parameters, as discussed in section 5.5, but in principle a factor-of-ten reduction in LLR measurement uncertainty over a timescale of years to a decade has the potential to deliver factor-of-ten improvements in LLR science.

Yet recent experience demonstrates that improving LLR measurement precision is not by itself sufficient to realize scientific gains. The model must also keep pace. Sections 5.3 and 5.4 provide a glimpse into the host of phenomena one must consider in plotting a course from centimeter-level to millimeter-level LLR accuracy. Progressing into the sub-millimeter regime will undoubtedly invoke a similarly sized—if not larger—list of concerns that may or may not be tractable. Even so, the aforementioned reflector/transponder upgrades would permit a greater global distribution of ever-improving LLR-capable stations, in addition to relieving the current burden on statistical reduction of the dominant tilt-induced timing uncertainty. Since many of the challenges confronting LLR today relate to Earth phenomenology, widespread global participation may be the best way to characterize these influences and reduce their impact on LLR science goals. Improved reflectors and/or transponders may provide the most robust route for future improvements in LLR science.

7. Conclusion

Since its inception, LLR has established itself as a mainstay of precision measurement relating to gravitation, physics of the Earth–Moon system, and coordinate systems. The basic measurement is general enough to have broad reach across many dimensions of physics. Within the gravity sector, LLR provides the very best probes of the equivalence principle, the time-rate-of-change of the gravitational constant, gravitomagnetism, geodetic precession, the inverse-square law, preferred-frame effects, and is also well positioned to test new ideas in physics. For the Earth–Moon system, dissipative processes in the lunar interior expose a liquid core, LLR measurements contribute to knowledge of Earth orientation

and coordinate systems, and tidal dissipation on Earth is seen via the egress of the lunar orbit.

Despite order-of-magnitude degradation of reflector signal strength, LLR data are now gathered at unprecedented rates and approaching 1 mm range precision as a consequence. Rediscovery of the long-lost Lunokhod 1 reflector brings the total available reflectors on the Moon up to five. At this time, the lunar reflectors are the limiting source of temporal uncertainty in the ranging error budget, so that new reflectors on the lunar surface would offer a dramatic improvement in range precision capability. Additionally, new reflectors or even transponders on the lunar surface could open up LLR to dozens of satellite laser ranging stations around the world, vastly improving data volume, global distribution, and interest in the science.

Alongside the challenge of acquiring accurate lunar range measurements, the sophisticated model that accounts for every relevant influence must see concomitant improvements. Currently in the process of adapting to millimeter-quality data after decades of centimeter-quality measurements, newly improved limits on science from LLR may be around the corner.

Acknowledgments

Some of the text in this article was adapted from proposals, to which Eric Adelberger, Christopher Stubbs, John Chandler, Duncan Agnew and David Crossley contributed. Some text has also been adapted from the author's direct contribution to the review article by Müller *et al* [3], which also includes U Schreiber, P J Shelus, J-M Torre, J G Williams, D H Boggs, S Boquillon and G Francou as co-authors. Some text is adapted from the APOLLO instrument paper [71], with co-authors E G Adelberger, J B R Battat, L N Carey, C D Hoyle, P LeBlanc, E L Michelsen, K Nordtvedt, A E Orin, J D Strasburg, C W Stubbs, H E Swanson and E Williams. Many of the results presented here reflect efforts by the same list of individuals associated with the APOLLO project. Nathan Johnson offered helpful comments. The author acknowledges funding support for lunar ranging and associated efforts by the National Science Foundation (Grant PHY-1068879), by NASA (NNX12AE96G and NNX10AU99G) and by the NASA Lunar Science Institute as part of the LUNAR consortium (NNA09DB30A).

Acronyms used in text

APD	avalanche photodiode
APOLLO	Apache Point Observatory Lunar Laser-ranging Operation
AU	astronomical unit (1.496×10^{11} m)
CfA	Harvard–Smithsonian Center for Astrophysics
CSR4	Center for Space Research ocean loading model 4
DGP	Dvali, Gabadadze, Porrati
DORIS	Doppler Orbitography and Radiopositioning Integrated by Satellite
EIH	Einstein–Infeld–Hoffmann
EP	Equivalence principle
FWHM	full-width and half-maximum
GOT00	Global Ocean Tide ocean loading model
GPS	Global Positioning System
GR	general relativity
GRACE	Gravity Recovery and Climate Experiment (Earth)
GRAIL	Gravity Recovery and Interior Laboratory (Moon)
ICRF	International Celestial Reference System
IERS	International Earth Rotation and Reference System Service
IMCCE	Institut de mecanique celeste et de calcul des ephemerides
JPL	Jet Propulsion Laboratory
LAGEOS	Laser Geodynamics Satellites
LLR	Lunar Laser Ranging
LOLA	Lunar Orbiter Laser Altimeter
LRO	Lunar Reconnaissance Orbiter
LUNAR	Lunar University Network for Astrophysical Research
MLRS	McDonald Laser Ranging System
NASA	National Aeronautics and Space Administration
OCA	Observatoire de la Côte d'Azur
PEP	Planetary Ephemeris Program
PPN	parametrized post Newtonian
RMS	root-mean-square
SBR	signal to background ratio
SEP	strong equivalence principle
SG	superconducting gravimeter
SLR	satellite laser ranging
SME	Standard Model Extension
SSB	solar system barycenter
TDC	time to digital converter
TPXO	TOPEX/Poseiden-based ocean loading model
UT1	Universal Time offset 1
UTC	Coordinated Universal Time
VLBI	very long baseline interferometry
WEP	weak equivalence principle
YAG	yttrium aluminum garnet

References

[1] Nordtvedt K Jr 1982 The fourth test of general relativity *Rep. Prog. Phys.* **45** 631–50

[2] Merkowitz S M 2010 Tests of gravity using lunar laser ranging *Living Rev. Relat.* **13** 7

[3] Müller J, Murphy T W Jr, Schreiber U, Shelus P J, Torre J-M, Williams J G, Boggs D H, Boquillon S and Francou G 2011 Lunar laser ranging—A tool for general relativity, lunar geophysics and Earth science *J. Geod.* submitted

[4] Williams J G, Turyshev S G and Boggs D H 2012 Lunar laser ranging tests of the equivalence principle *Class. Quantum Grav.* **29** 184004

[5] Müller J, Hofmann F and Biskupek L 2012 Testing various facets of the equivalence principle using lunar laser ranging *Class. Quantum Grav.* **29** 184006

[6] Müller J and Biskupek L 2007 Variations of the gravitational constant from lunar laser ranging data *Class. Quantum Grav.* **24** 4533–8

[7] Williams J G, Turyshev T G and Boggs D H 2004 Progress in lunar laser ranging tests of relativistic gravity *Phys. Rev. Lett.* **93** 261101 (arXiv:gr-qc/0411113)

[8] Hofmann F, Müller J and Biskupek L 2010 Lunar laser ranging test of the Nordtvedt parameter and a possible variation of the gravitational constant *Astron. Astrophys.* **522** L5

[9] Murphy T W Jr, Nordtvedt, K and Turyshev S G 2007 Gravitomagnetic influence on gyroscopes and on the lunar orbit *Phys. Rev. Lett.* **98** 071102 (arXiv:gr-qc/0702028)

[10] Soffel M, Klioner S, Müller J and Biskupek L 2008 Gravitomagnetism and lunar laser ranging *Phys. Rev.* D **78** 024033

[11] Müller J, Williams J G, Turyshev S G and Shelus P J 2006 Potential capabilities of lunar laser ranging for geodesy and relativity *Dynamic Planet* ed P Tregoning and C Rizos *I.A.G. Symposium (Cairns)* vol 130 pp 903–9

[12] Adelberger E G, Heckel B R and Nelson A E 2003 Tests of the gravitational inverse-square law *Annual Rev. Nucl. Part. Sci.* **53** 77–121 (arXiv:hep-ph/0307284)

[13] Williams J G, Boggs D H, Yoder C F, Ratcliff J T and Dickey J O 2001 Lunar rotational dissipation in solid body and molten core *J. Geophys. Res.* **106** 27933–68

[14] Khan A, Mosegaard K, Williams J G and Lognonne P 2004 Does the Moon possess a molten core? Probing the deep lunar interior using results from LLR and Lunar Prospector *J. Geophys. Res.* **109** E09007

[15] Müller J, Nordtvedt K and Vokrouhlicky D 1996 Improved constraint on the α_1 PPN parameter from lunar motion *Phys. Rev.* D **54** R5927–30

[16] Nordtvedt K 1987 Probing gravity to the second post-Newtonian order and to one part in 10^7 using the spin axis of the Sun *Astrophys. J.* **320** 871–4

[17] Nordtvedt K 2001 Testing Newton's third law using lunar laser ranging *Class. Quantum Grav.* **18** L133

[18] Lue A and Starkman G 2003 Gravitational leakage into extra dimensions: probing dark energy using local gravity *Phys. Rev.* D **67** 064002 (arXiv:astro-ph/0212083)

[19] Dvali G, Gruzinov A and Zaldarriaga M 2003 The accelerated Universe and the Moon *Phys. Rev.* D **68** 024012 (arXiv:hep-ph/0212069)

[20] Williams J G, Turyshev S G and Boggs D H 2009 Lunar laser ranging tests of the equivalence principle with the Earth and Moon *Int. J. Mod. Phys.* D **18** 1129–75

[21] Baeßler S, Heckel B R, Adelberger E G, Gundlach J H, Schmidt U and Swanson H E 1999 Improved test of the equivalence principle for gravitational self-energy *Phys. Rev. Lett.* **83** 3585

[22] Dickey J O *et al* 1994 Lunar laser ranging: a continuing legacy of the Apollo program *Science* **265** 482

[23] Murphy T W Jr, Adelberger E G, Battat J B R, Hoyle C D, McMillan R J, Michelsen E L, Samad R L, Stubbs C W and Swanson H E 2010 Long-term degradation of optical devices on the Moon *Icarus* **208** 31–5 (arXiv:1003.0713)

[24] Moyer T D 1981 Transformation from proper time on earth to coordinate time in solar system barycentric space-time frame of reference: I *Celest. Mech.* **23** 33–56
Moyer T D 1981 Transformation from proper time on earth to coordinate time in solar system barycentric space-time frame of reference: II *Celest. Mech.* **23** 57–68

[25] Williams J G, Newhall X X and Dickey J O 1996 Relativity parameters determined from lunar laser ranging *Phys. Rev.* D **53** 6730

[26] Müller J, Soffel M and Klioner S 2008 Geodesy and relativity *J. Geod.* **82** 133–45

[27] de Bernardis P *et al* 2000 A flat Universe from high-resolution maps of the cosmic microwave background radiation *Nature* **404** 955 (arXiv:astro-ph/0004404)

[28] Hanany S *et al* 2000 MAXIMA 1: a measurement of the cosmic microwave background anisotropy on angular scales of $10'$–$5''$ *Astrophys. J.* **545** L5 (arXiv:astro-ph/0005123)

[29] Netterfield C B *et al* 2002 A measurement by BOOMERANG of multiple peaks in the angular power spectrum of the cosmic microwave background *Astrophys. J.* **571** 604 (arXiv:astro-ph/0104460)

[30] Pryke C, Halverson N W, Leitch E M, Kovac J, Carlstrom J E, Holzapfel L and Dragovan M 2002 Cosmological parameter extraction from the first season of observations with DASI *Astrophys. J.* **568** 46 (arXiv:astro-ph/0104490)

[31] Komatsu E *et al* 2009 *Astrophys. J. Suppl. Ser.* **180** 330–76 (arXiv:0803.0547)

[32] Perlmutter S *et al* 1999 Measurements of omega and lambda from 42 high-redshift supernovae *Astrophys. J.* **517** 565 (arXiv:astro-ph/9812133)

[33] Riess A *et al* 1998 Observational evidence from supernovae for an accelerating Universe and a cosmological constant *Astron. J.* **116** 1009 (arXiv:astro-ph/9805201)

[34] Peacock J A *et al* 2001 A measurement of the cosmological mass density from clustering in the 2dF galaxy redshift survey *Nature* **410** 169 (arXiv:astro-ph/0103143)

[35] Eisenstein D J *et al* 2005 Detection of the baryon acoustic peak in the large-scale correlation function of SDSS luminous red galaxies *Astrophys. J.* **633** 560–74 (arXiv:astro-ph/0501171)

[36] Damour T 1996 Testing the equivalence principle: why and how? *Class. Quantum Grav.* **13** A33 (arXiv:gr-qc/9606080)

[37] Damour T and Vokrouhlicky D 1996 Equivalence principle and the Moon *Phys. Rev.* D **53** 4177 (arXiv:gr-qc/9507016)

[38] Nordtvedt K 1968 Testing relativity with laser ranging to the Moon *Phys. Rev.* **170** 1186

[39] Nordtvedt K 1968 Equivalence principle for massive bodies: I. Phenomenology *Phys. Rev.* **169** 1014

[40] Nordtvedt K 1968 Equivalence principle for massive bodies: II. Theory *Phys. Rev.* **169** 1017

[41] Nordtvedt K 1995 The relativistic orbit observables in lunar laser ranging *Icarus* **114** 51

[42] Damour T and Nordtvedt K 1993 Tensor-scalar cosmological models and their relaxation toward general relativity *Phys. Rev.* D **48** 3436

[43] Gonzalez M E *et al* 2011 High-precision timing of five millisecond pulsars: space velocities, binary evolution, and equivalence principles *Astrophys. J.* **743** 102

[44] Freire P C C, Kramer M and Wex N 2012 Tests of the universality of free fall for strongly self-gravitating bodies with radio pulsars *Class. Quantum Grav.* **29** 184007

[45] Steinhardt P J and Wesley D 2010 Exploring extra dimensions through observational tests of dark energy and varying Newton's constant (arXiv:1003.2815v1)

[46] Verbiest J P W, Bailes M, van Straten W, Hobbs G B, Edwards R T, Manchester R N, Bhat N D R, Sarkissian J M, Jacoby B A and Kulkarni S R 2008 Precision timing of PSR J04374715: an accurate pulsar distance, a high pulsar mass, and a limit on the variation of Newton's gravitational constant *Astrophys. J.* **679** 675

[47] Freire P C C, Wex N, Esposito-Farese J, Verbiest J P W, Bailes M, Jacoby B A, Kramer M, Stairs I H, Antoniadis J and Janssen G H 2012 The relativistic pulsar-white dwarf binary PSR J1738+0333: II. The most stringent test of scalar-tensor gravity *Mon. Not. R. Astron. Soc.* **423** 3328

[48] Nordtvedt K and Will C M 1972 Conservation laws and preferred frames in relativistic gravity: II. Experimental evidence to rule out preferred-frame theories of gravity *Astrophys. J.* **177** 775–92

[49] Will C M 1993 *Theory and Experiment in Gravitational Physics* (New York: Cambridge University Press)

[50] Bertotti B, Iess L and Tortora P 2003 A test of general relativity using radio links with the Cassini spacecraft *Nature* **425** 374–6

[51] Everitt C F W *et al* 2011 Gravity probe B: final results of a space experiment to test general relativity *Phys. Rev. Lett.* **106** 221101

[52] Ciufolini I, Paolozzi A, Pavlis E C, Ries J C, Koenig R, Matzner R A, Sindoni G and Neumayer H 2009 Towards a one percent measurement of frame dragging by spin with satellite laser ranging to LAGEOS, LAGEOS 2 and LARES and GRACE gravity models *Space Sci. Rev.* **148** 71–104

[53] Iorio L 2009 An assessment of the systematic uncertainty in present and future tests of the Lense–Thirring effect with satellite laser ranging *Space Sci. Rev.* **148** 363–81

[54] Kopeikin S M 2007 Comment on 'Gravitomagnetic influence on gyroscopes and on the lunar orbit' *Phys. Rev. Lett.* **98** 229001

[55] Ciufolini I 2010 Frame-dragging, gravitomagnetism and lunar laser ranging *New Astron.* **15** 332–7

[56] Murphy T W Jr 2009 Lunar ranging, gravitomagnetism, and APOLLO *Space Sci. Rev.* **148** 217–23

[57] Breton R P, Kaspi V M, Kramer M, McLaughlin M A, Lyutikov M, Ransom S M, Stairs I H, Ferdman R D, Camilo F and Possenti A 2008 Relativistic spin precession in the double pulsar *Science* **321** 104

[58] Dvali G, Gabadadze G and Shifman M 2003 Diluting cosmological constant in infinite volume extra dimensions *Phys. Rev.* D **67** 044020 (arXiv:hep-th/0202174)

[59] Colladay D and Kostelecky V A 1998 Lorentz-violating extension of the standard model *Phys. Rev.* D **58** 116002

[60] Kostelecky V A 2004 Gravity, Lorentz violation, and the standard model *Phys. Rev.* D **59** 105009

[61] Bailey Q G and Kostelecky V A 2006 Signals for Lorentz violation in post-Newtonian gravity *Phys. Rev.* D **74** 045001

[62] Battat J B R, Chandler J F and Stubbs C W 2007 Testing for Lorentz violation: constraints on standard-model-extension parameters via lunar laser ranging *Phys. Rev. Lett.* **99** 241103

[63] Williams J G, Newhall X X and Dickey J O 1996 Lunar moments, tides, and coordinate frames *Planet. Space Sci.* **44** 1077–80

[64] Rambaux N and Williams J G 2011 The Moon's physical librations and determination of their free modes *Celest. Mech. Dyn. Astron.* **109** 85–100

[65] Williams J G and Boggs D H 2009 What does LLR see? *Proc. 16th Int. Workshop on Laser Ranging (Ponzan)* vol 1 pp 101–120

[66] Biskupek L and Müller J 2009 Relativity and Earth orientation parameters from lunar laser ranging *Proc. 16th Int. Workshop on Laser Ranging (Ponzan)* vol 1 p 270–6

[67] Petit G and Luzum B (ed) 2010 *IERS Conventions (2010)*, *IERS Technical Note*, No 36

[68] Bender P L *et al* 1973 The lunar laser ranging experiment *Science* **182** 229

[69] Samain E *et al* 1998 Millimetric lunar laser ranging at OCA *Astron. Astrophys. Suppl. Ser.* **130** 235

[70] Shelus P J 1985 MLRS: a lunar/artificial satellite laser ranging facility at the McDonald observatory *IEEE Trans. Geosci. Remote Sensing* **GE-23** 385

[71] Murphy T W Jr *et al* 2008 The Apache Point Observatory Lunar Laser-ranging Operation: instrument description and first detections *Publ. Astron. Soc. Pacific* **120** 20–37 arXiv:0710.0890.

[72] Battat J B R *et al* 2009 The Apache Point Observatory Lunar Laser-ranging Operation (APOLLO): two years of millimeter-precision measurements of the Earth–Moon range *Publ. Astron. Soc. Pacific* **121** 29–40

[73] Murphy T W Jr, Adelberger E G, Battat J B R, Hoyle C D, Johnson N H, McMillan R J, Stubbs C W and Swanson H E 2012 APOLLO: millimeter lunar laser ranging *Class. Quantum Grav.* **29** 184005

[74] Stooke P J 2005 Lunar laser ranging and the location of lunokhod 1 *Lunar and Planetary Institute Technical Rep. 36th Annual Lunar and Planetary Science Conf.* (League City, TX) vol 36 ed S Mackwell and E Stansbery paper 1194

[75] Murphy T W Jr, Adelberger E G, Battat J B R, Hoyle C D, Johnson N H, McMillan R J, Michelsen E L, Stubbs C W and Swanson H E 2011 Laser ranging to the lost Lunokhod 1 reflector *Icarus* **211** 1103–8

[76] Murphy T W, Adelberger E G, Battat J B, Hoyle C D, Michelsen E L, Stubbs C W and Swanson H E 2006 Absolute calibration of LLR signal: Reflector health status *Proc. 15th Int. Workshop on Laser Ranging (Canberra, Australia, October 2006)* vol 2 pp 540–5

[77] Goodrow S D and Murphy T W Jr 2012 Effects of thermal gradients on total internal reflection corner cubes *Appl. Opt.* **51** 8793–9

[78] Stubbs T J, Vondrak R R and Farrell W M 2006 A dynamic fountain model for lunar dust *Adv. Space Res.* **37** 59–66

[79] Farrell W M, Stubbs T J, Vondrak R R, Delory G T and Halekas J S 2007 Complexelectric fields near the lunar terminator: the near-surface wake and accelerated dust *Geophys. Res. Lett.* **34** L14201

[80] www.ecgs.lu/ggfc/

[81] Tregoning P and van Dam T 2005 Atmospheric pressure loading corrections applied to GPS data at the observation level *Geophys. Res. Lett.* **32** L22310

[82] Ramillien G, Famiglietti S and Wahr J 2008 Detection of continental hydrology and glaciology signals from GRACE: a review *Surv. Geophys.* **29** 361–74

[83] Chen J L, Wilson C R, Eanes R J and Nerem R S 1999 Geophysical interpretation of observed geocenter variation *J. Geophys. Res.—Solid Earth* **104** 2683

[84] Cretaux J F, Soudarin L, Davidson F J M, Gennero M C, Berge-Nguyen M and Cazenave A 2002 Seasonal and interannual geocenter motion from SLR and DORIS measurements: comparison with surface loading data *J. Geophys. Res.—Solid Earth* **107** 2374

[85] Lavallee D A, van Dam T, Blewitt G and Clarke P J 2006 Geocenter motions from GPS: a unified observation model *J. Geophys. Res.—Solid Earth* **111** B05405

[86] Vokrouhlicky D 1997 A Note on the solar radiation perturbations of lunar motion *Icarus* **126** 293

[87] Mendes V B and Pavlis E C 2004 High-accuracy zenith delay prediction at optical wavelengths *Geophys. Res. Lett.* **31** L14602

[88] Mendes V B, Prates G, Pavlis E C, Pavlis D E and Langley R B 2002 Improved mapping functions for atmospheric refraction correction in SLR *Geophys. Res. Lett.* **29** 1414

[89] Hulley G and Pavlis E C 2006 Improvement of current refraction modeling in satellite laser ranging (SLR) by ray tracing through meteorological data *Proc. 15th Int. Workshop on Laser Ranging (Canberra)* vol 2 p 345

[90] Preston A, Thorpe J I and Miner L 2012 Quasi-monolithic structures for spaceflight using hydroxide-catalysis bonding *IEEE Aerospace Conf. (Big Sky, MT)*

[91] Currie D, Dell'Agnello S and Monache G D 2011 A lunar laser ranging retroreflector array for the 21st Century *Acta Astron.* **68** 667

[92] Turyshev S G, Farr W, Folkner W M, Girerd A R, Hemmati H, Murphy T W Jr, Williams J G and Degnan J J 2010 Advancing tests of relativistic gravity via laser ranging to Phobos *Exp. Astron.* **28** 209–49